On helium-dominated stellar evolution:
the mysterious role of the O(He)-type stars ★, ★★, ★★★

N. Reindl[1], T. Rauch[1], K. Werner[1], J. W. Kruk[2], and H. Todt[3]

[1] Institute for Astronomy and Astrophysics, Kepler Center for Astro and Particle Physics, Eberhard Karls University, Sand 1, 72076 Tübingen, Germany
e-mail: reindl@astro.uni-tuebingen.de
[2] NASA Goddard Space Flight Center, Greenbelt, MD 20771, USA
[3] Institute for Physics and Astronomy, University of Potsdam, Karl-Liebknecht-Str. 24/25, 14476 Potsdam, Germany

ABSTRACT

Context. About a quarter of all post-asymptotic giant branch (AGB) stars are hydrogen-deficient. Stellar evolutionary models explain the carbon-dominated H-deficient stars by a (very) late thermal pulse scenario where the hydrogen-rich envelope is mixed with the helium-rich intershell layer. Depending on the particular time at which the final flash occurs, the entire hydrogen envelope may be burned. In contrast, helium-dominated post-AGB stars and their evolution are yet not understood.

Aims. A small group of very hot, helium-dominated stars is formed by O(He)-type stars. A precise analysis of their photospheric abundances will establish constraints to their evolution.

Methods. We performed a detailed spectral analysis of ultraviolet and optical spectra of four O(He) stars by means of state-of-the-art non-LTE model-atmosphere techniques.

Results. We determined effective temperatures, surface gravities, and the abundances of H, He, C, N, O, F, Ne, Si, P, S, Ar, and Fe. By deriving upper limits for the mass-loss rates of the O(He) stars, we found that they do not exhibit enhanced mass-loss. The comparison with evolutionary models shows that the status of the O(He) stars remains uncertain. Their abundances match predictions of a double helium white dwarf merger scenario, suggesting that they might be the progeny of the compact and of the luminous helium-rich sdO-type stars. The existence of planetary nebulae that do not show helium enrichment around every other O(He) star, precludes a merger origin for these stars. These stars must have formed in a different way, for instance via enhanced mass-loss during their post-AGB evolution or a merger within a common-envelope (CE) of a CO-WD and a red giant or AGB star.

Conclusions. A helium-dominated stellar evolutionary sequence exists, that may be fed by different types of mergers or CE scenarios. It appears likely, that all these pass through the O(He) phase just before they become white dwarfs.

Key words. stars: evolution – stars: abundances – stars: fundamental parameters – stars: AGB and post-AGB

1. Introduction

Quantitative spectral analyses of hot, post-asymptotic giant branch (AGB) stars revealed two distinct evolutionary sequences. Besides the well understood H-rich sequence, a H-deficient sequence was discovered. It is composed of Wolf-Rayet-type stars that evolve into PG 1159-type stars and finally might evolve into non-DA white dwarfs (WDs). While (very) late thermal pulse ((V)LTP) evolutionary models can explain the observed He, C, and O abundances in these stars (the typical abundance pattern for PG 1159 stars is He : C : O = $0.30 - 0.85 : 0.15 - 0.60 : 0.02 - 0.20$ by mass, Werner & Herwig 2006) they do not reproduce the abundances in He-dominated stars, such as subdwarf O (sdO) stars, R Coronae Borealis (RCB) stars, extreme helium (EHe) stars, and the O(He) stars.

Two evolutionary scenarios for the origin of RCB and EHe stars were suggested. They might either be formed by a final He-shell flash or be the merger product of a CO WD with a He WD (Jeffery et al. 2011). The significant Li content in the atmospheres of RCB stars supports the idea of an LTP to explain their origin. However, the relatively high inferred masses of RCB stars and their high F abundance supports a WD merger (Clayton et al. 2011). Zhang & Jeffery (2012a) suggested that a double He-WD merger might also explain RCB and EHe stars. Recently, Kameswara Rao et al. (2013) found the RCB star DY Cen to be the first and only binary system among the RCB stars and their probable relatives. DY Cen is one of the hottest and most H-rich members of the RCB stars. Kameswara Rao et al. (2013) suggested that this system might have evolved from a common-envelope system to its current form. Therefore it may be possible that RCB stars form in various ways.

RCB and EHe stars are not the only He-rich stars for which a merger origin was suggested. Zhang & Jeffery (2012b) presented the results of a double He-WD merger to explain the formation of He-rich, hot sdOs. These can be divided into three subgroups, one C-rich and N-poor, the other N-rich and C-poor, and the third one enriched in C and N (Hirsch 2009). In their

---

numerical experiments, Zhang & Jeffery (2012b) showed that in terms of T_{eff}, $\log g$, C, and N abundances, the origin of the two sdO groups can be explained by different double He-WD merger models. Zhang & Jeffery (2012b) distinguished between three types of mergers. In a slow-merger process the less massive He WD transfers its entire mass within a few minutes to form a disk around the primary He WD, which then accretes from it at a rate similar to the Eddington-accretion rate. The surface composition of the resulting star retains the N-rich composition of the accreted WD. In the fast-merger model, the secondary directly transfers its entire mass quickly to the primary surface, where heating up to 10^8 K causes the material to expand and form a hot corona within a few minutes. The fast-merger model produces C-rich stars, in which N is hardly observable. The composite merger includes both processes. In general, models with a merged mass below 0.7 $M_\odot$ produce an N-rich star, while more massive ones produce a C-rich star with a significant N content. Other origins of He-rich sdO stars are discussed as well. Because the merger of a He WD with a post-sdB star is predicted in one of the important binary channels for the formation of sdB stars (Han et al. 2002, 2003), Justham et al. (2011) proposed this formation channel for the previously unexplained He-rich sdO stars. Their models also reproduced the properties of the He-rich sdO stars in terms of T_{eff} and $\log g$. However, in contrast to Zhang & Jeffery (2012b), they did not include nuclear evolution in their calculations.

A more exotic group of He-dominated stars is formed by the O(He) stars. This spectroscopic class is defined by an almost pure He II absorption-line spectrum in the optical wavelength range (Méndez et al. 1986; Rauch et al. 1998). For more than 15 years, only the two central stars of planetary nebulae (CSPNe) K 1−27[1] (WD 0558−756) and LoTr 4, as well as HS 1522+6615 (WD 1522+662), and HS 2209+8229 (WD 2209−8229) were known (Rauch et al. 1994, 1996, 1998). Recently, Werner et al. (2014) found four more of these objects, namely SDSS J 172854.34+361958.62, SDSS J 171916.97+365326.70, SDSS J 141812.50+024426.92, and SDSS J 075732.18+184329.28. They also pointed out that KPD 0005+5106 is a pre-WD. Because of the He-rich surface composition of KPD 0005+5106 (98% by mass, Wassermann et al. 2010), we also consider it as an O(He) star. The evolutionary status of these objects has been studied only rarely. Rauch et al. (1998) proposed that O(He) stars might be succesors of the luminous He-rich sdO stars and that because of due ongoing mass loss, the low-gravity O(He) stars might envolve into PG 1159 stars. This possibility was studied by Miller Bertolami & Althaus (2006). They had to assume mass-loss rates, that were higher than predicted by radiation-driven wind theory, to turn O(He) stars into helium-enriched PG 1159 stars. An alternative scenario was suggested by Rauch et al. (2006). They invoked the idea that the O(He) stars could also be the offspring of a merging event of two white dwarfs and thus, the direct descendants of RCB stars.

In this paper, we present the analysis of K 1−27, LoTr 4, HS 1522+6615, and HS 2209+8229. In Sect. 2, we briefly describe the available observations. We then present a detailed spectral analysis of the O(He) stars based on optical and ultraviolet spectra (Sect. 3) and derive stellar parameters and distances (Sect. 4). In Sect. 5 we discuss possible evolutionary channels for the O(He) stars and those of other helium-dominated objects. We conclude in Sect. 5.3.

2. Observations

In January, June and July 2013, we performed observations of K 1−27 and LoTr 4 with the ESO/NTT (ProgIDs 091.D-0663, 090.D-0626) using the EFOSC2 spectrograph (resolving power $R = \lambda/\Delta\lambda \approx 3000$) with the grisms GR#19 (4400 to 5100 Å) and GR#20 (6000 to 7100 Å). The data reduction was done by using IRAF[2]. The previous optical spectra of the O(He) stars were already described and analyzed by Rauch et al. (1994, 1996, 1998) to determine effective temperature (T_{eff}), surface gravity ($\log g$), and the H/He ratio for all four stars as well as the C abundance for K 1−27, LoTr 4 (upper limits), HS 1522+6615, and the N abundance for K 1−27 and LoTr 4.

We have taken FUV spectra with FUSE[3] ($R \approx 20000$) in 2002 (all O(He) stars, 49 ksec exposure time in total, ProgID: C178) and 2005 (only HS 1522+6615, 4 ksec, ProgID: U103) using the LWRS aperture (Figs. 1 − 4). Additional 204 ksec of FUSE observations (K 1−27, HS 1522+6615, HS 2209+8229) were scheduled for summer 2007, but were not be performed because of the FUSE failure on July 12. The FUSE spectra show a strong contamination by interstellar (IS) line absorption and the S/N ratio is very poor (Rauch et al. 2006, 2009). To reduce the pixel-to-pixel variation, they were co-added and then slightly smoothed with a low-pass filter (Savitzky & Golay 1964).

Because of the poor quality of the FUSE spectra, we obtained HST/COS[4] spectra (Proposal Id: 11699, Figs. 5 − 8) during April to July 2010 using the grating G140L ($2000 < R < 3500$ within 1150 Å $< \lambda < 1800$ Å) and the primary science aperture.

3. Spectral analysis

Motivated by the new COS spectra, we decided to comprehensively re-analyze all available data of the O(He) stars. Since the time when Rauch et al. (1998) presented their analysis of optical, ultraviolet (IUE[5]), and X-ray (ROSAT[6]) data, our Tübingen NLTE Model Atmosphere Package TMAP[7] (Sect. 3.1) as well as the atomic data, that is taken from TMAD[8], the Tübingen Model Atom Database, have continuously improved. Moreover, in a standard procedure, we modeled photospheric and interstellar line-absorption spectra to correctly identify the pure atmospheric lines. Absorption by interstellar gas was modeled using the program Owens (Hébrard & Moos 2003; Hébrard et al. 2002). Owens allows for multiple independent interstellar clouds, each with its own radial and turbulent velocities, temperature, and column densities for each of any number of constituent gas species. All properties of each cloud are adjusted by fitting Voigt profiles to the data by chi-squared minimization.

3.1. Model atmospheres

We used TMAP (Werner et al. 2003; Rauch & Deetjen 2003) to compute plane-parallel, line-blanketed non-LTE model atmospheres in radiative and hydrostatic equilibrium. In the previous analysis of the O(He) stars, Rauch et al. (1994, 1996, 1998)

---

[1] In the following, we use the PNe names to identify their central stars.

[2] IRAF is distributed by the National Optical Astronomy Observatory, which is operated by the Associated Universities for Research in Astronomy, Inc., under cooperative agreement with the National Science Foundation.

[3] Far Ultraviolet Spectroscopic Explorer

[4] Cosmic Origins Spectrograph

[5] International Ultraviolet Explorer

[6] Röntgensatellit

[7] http://astro.uni-tuebingen.de/~TMAP

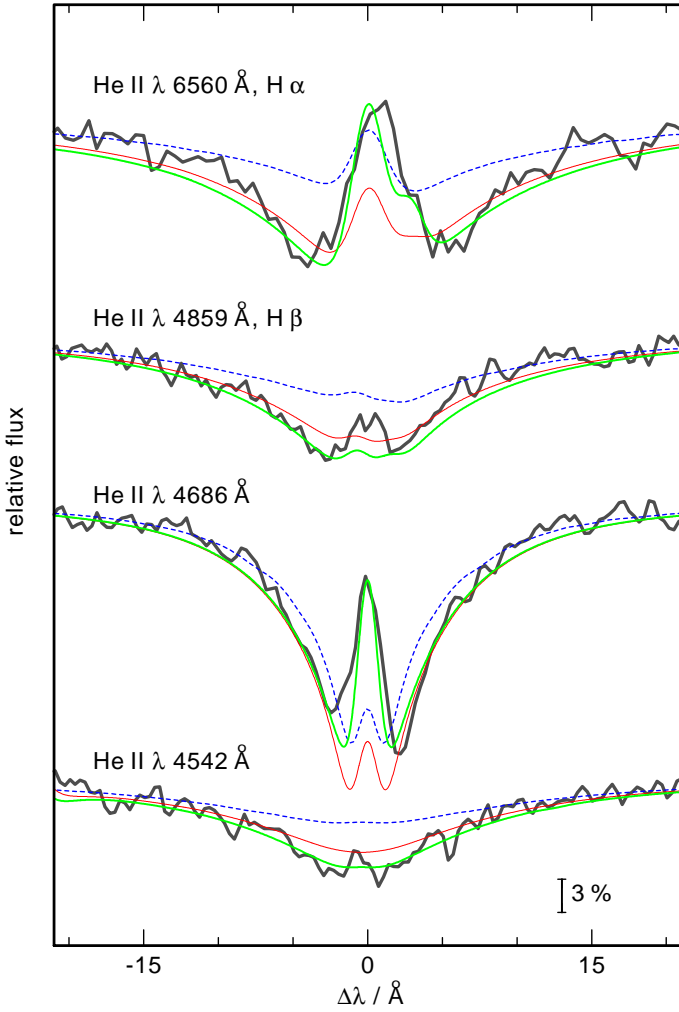[8] http://astro.uni-tuebingen.de/~TMAD

Fig. 13. Comparison of optical H I and He II lines calculated from models including H+He (dashed, blue), H+He+C+N+O (thin, red), and H+He+C+N+O+Ne (thick, green) with $T_{\rm eff} = 135$ kK and $\log g = 6.4$, overplotted on the EFOSC2 spectrum of K 1−27. The vertical bar indicates 3 % of the continuum flux.

Fig. 14. Determination of the interstellar H I column density toward K 1−27. The dashed lines indicate the error limits. The thin (blue) line is the pure photospheric spectrum. Prominent spectral lines are marked at top, "is" indicates interstellar origin. The line center of Ly α is dominated by geocoronal emission.

Fig. 15. Determination of $E_{B−V}$ for HS 1522+6615. The FUSE and COS spectra and GALEX and BVR brightnesses from the GSC 2.3 catalog are used for comparison. The thick (blue) line is the spectrum of the final photospheric model. The dashed lines indicate the error limits.

used only H+He model atmospheres to derive $T_{\rm eff}$, $\log g$, and the H/He ratio. In our analysis, we also included the elements C, N, O, F, Ne, Si, P, S, and Ar with their dominant ionization stages (Table 1, Figs. 9 − 12) to study their impact on the model atmospheres and the resulting line profiles. We found that C, N, O, and Ne have a strong influence on the atmospheric structure. In Fig. 13 we demonstrate the strong effect of additional opacities on the resulting line profiles. The impact of F, Si, P, S, and Ar turned out to be negligible. Dreizler & Werner (1994) have shown that line blanketing by iron-group elements hardly affects the hydrogen and helium lines in hot central stars. To compute a model grid in reasonable time, we therefore decided to include only H, He, C, N, O, and Ne in our model atmospheres to derive $T_{\rm eff}$, $\log g$, and the element abundances of these elements. To determine the abundances of F, Si, P, S, Ar, and Fe, we kept the values of $T_{\rm eff}$ and $\log g$ fixed. The upper limits (Table 3) were derived by test models where the respective lines in the model contradict the non-detection of the lines in the observation (at the abundance limit).
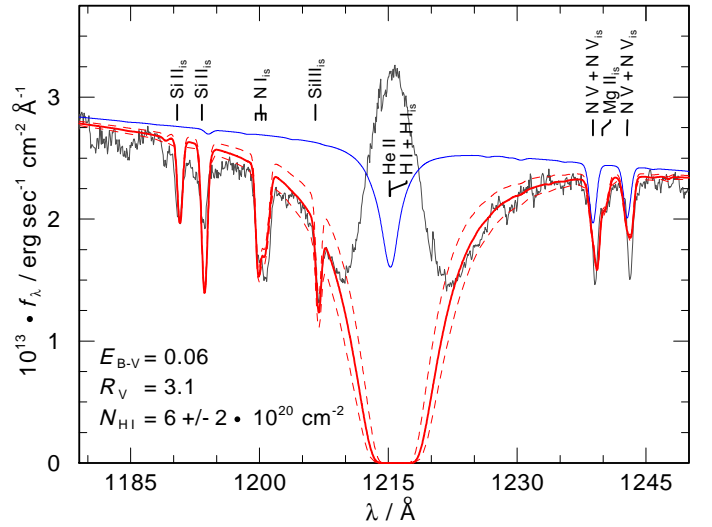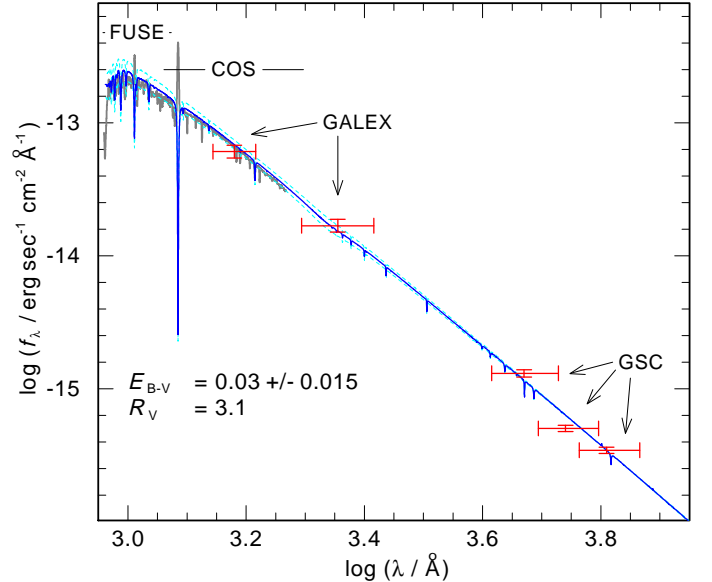
3.2. Interstellar neutral hydrogen and reddening

The interstellar H I column density was measured from Ly α (Fig. 14). Interstellar reddening was determined using the reddening law of Fitzpatrick (1999). Since its impact is negligible in the infrared, the model flux was normalized to the most reddest brightness found in the literature. Fig. 15 shows the example of HS 1522+6615, where the GSC[9] R brightness is used. Table 2 summarizes $N_{\rm HI}$ and $E_{B−V}$ of the O(He) stars compared with GALEX[10] values, which agree well. Within the error limits, our values agree with those of Rauch et al. (1998).

---

[9] Guide Star Catalogue, Bucciarelli et al. (2001)
[10] Galaxy Evolution Explorer, http://www.galex.caltech.edu/

Table 2. Interstellar H I column density and reddening.

| object | $N_{\mathrm{H\,I}}\,[10^{20}\mathrm{cm}^{-2}]$ | E_{B-V} | |
		this work	GALEX
K 1−27	6.0 ± 2.0	0.06 ± 0.020	0.0797
LoTr 4	10.0 ± 1.5	0.20 ± 0.020	0.1893
HS 1522+6615	2.0 ± 1.0	0.03 ± 0.015	0.0250
HS 2209+8229	5.0 ± 1.0	0.23 ± 0.040	
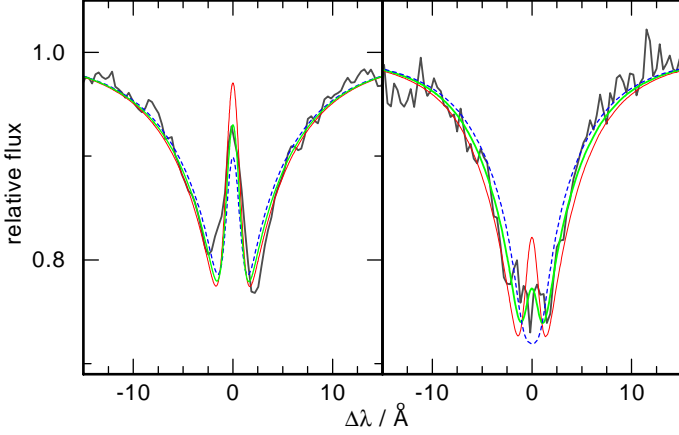
Fig. 16. Determination of T_{eff} of K 1−27 (left) and LoTr 4 (right) using the central emission of He II $\lambda\,4686$ Å. The EFOSC2 observation (solid black line) is compared with models with T_{eff} = 130/110 kK (dashed, blue), 135/120 kK (thick, green), and 140/130 kK (thin, red).

3.3. Effective temperature and surface gravity

To determine of T_{eff} and $\log g$, we used the optical H I and He II lines. For HS 1522+6615 and HS 2209+8229 we additionally used the O ionization equilibria to constrain T_{eff}. The new optical observation of K 1−27 and LoTr 4 allowed us to use the central emission of He II $\lambda\,4686$ Å to derive T_{eff} for the two CSPNe (Fig. 16).

For K 1−27, T_{eff} = 135 kK and $\log g$ = 6.4 (cm/s) were found. The value of $\log g$ agrees with Rauch et al. (1994, 1998, $\log g = 6.5 \pm 0.5$), but for T_{eff} we found a large deviation from the result of Rauch et al. (1998, T_{eff} = 105 ± 10 kK). However, Rauch et al. (1994, 1998) encountered problems with the lower value of T_{eff} which can be solved with T_{eff} = 135 kK: first, with T_{eff} = 105 kK the star did not provide enough hard photons to ionize its nebula. With the higher T_{eff} for K 1−27, we achieve a more consistent PN ↔ CSPN model. Second, N V $\lambda\lambda\,4604, 4620$ Å do not appear in emission at T_{eff} = 105 kK (as the observation shows), but for T_{eff} = 135 kK they do. Finally, Rauch et al. (1994) had the problem that the central depression of the He II $\lambda\,4686$ Å (n − n' = 3 − 4) line was too strong, while other H I and He II lines were almost perfectly reproduced. The addition of Ne to the models solves this problem. Furthermore, the central He II $\lambda\,4686$ Å and H α emission can only be reproduced with a supersolar Ne abundance, which causes a strong decrease of the temperature in the outer atmosphere. He II $\lambda\,4686$ Å and H α are most affected by this because they are formed at lower Rosseland optical depths. We stress that the large deviation from the previous T_{eff} value is a result of the additional opacities used in our model atmospheres, as mentioned above.

For LoTr 4, we confirmed the value of T_{eff} = 120 kK (Rauch et al. 1996) but increased the lower limit to T_{eff} = 115 kK because for lower values, N V $\lambda\lambda\,4604, 4620$ Å do not appear in
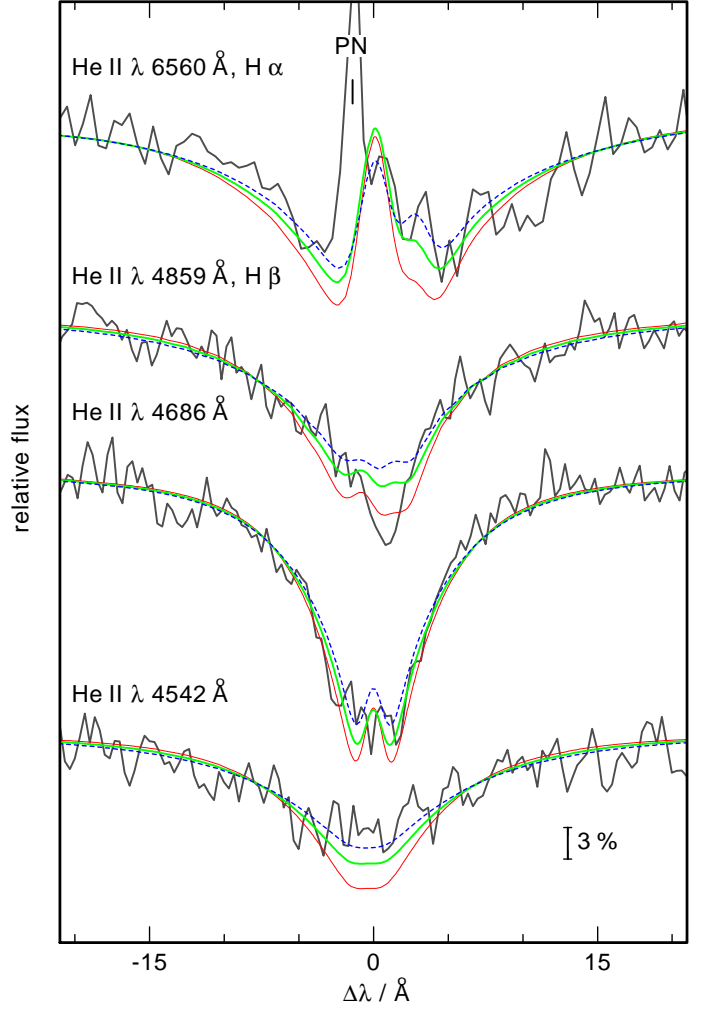
Fig. 17. Determination of $\log g$ of LoTr 4. The EFOSC2 observation (solid black line) is compared with models with $\log g$ = 6.0 (dashed, blue), 5.8 (thick, green), and 5.6 (thin, red). The vertical bar indicates 3 % of the continuum flux.

emission as in the observation. The new optical spectra allowed us a better determination of the surface gravity (Fig. 17). We found $\log g = 5.8 \pm 0.2$, which is within the error limits of the literature value (Rauch et al. 1996, $\log g = 5.5 \pm 0.5$).

For HS 1522+6615, we determined a lower value of T_{eff} = 130 kK at a higher $\log g$ = 5.9 (compared with Rauch et al. 1998, T_{eff} = 140 ± 10 kK, $\log g = 5.5 \pm 0.5$). The errors of $\log g$ were reduced to ± 0.2.

Based on the O IV / O V ionization equilibrium (Fig. 18), we found a higher T_{eff} = 110 kK compared with the literature value (T_{eff} = 100 ± 10 kK) for HS 2209+8229. The value of $\log g$ = 6.0 is verified and the errors were reduced to ± 0.3.

3.4. Element Abundances

The H/He abundance ratio (by mass) was determined using H I $\lambda\lambda\,6563, 4861, 4340$ Å and He II $\lambda\lambda\,6560, 5412, 4859, 4686, 4542, 4339$ Å. It was difficult to fix because the quality of the available optical observations is poor. For LoTr 4 and K 1−27, we reverified the literature values of 0.5 and 0.2, respectively. Fig. 19 shows that for HS 1522+6615 the model with H/He = 0.03 fits the observation better than H/He = 0.10 (literature value) where H α appears in emission while for H/He = 0.01
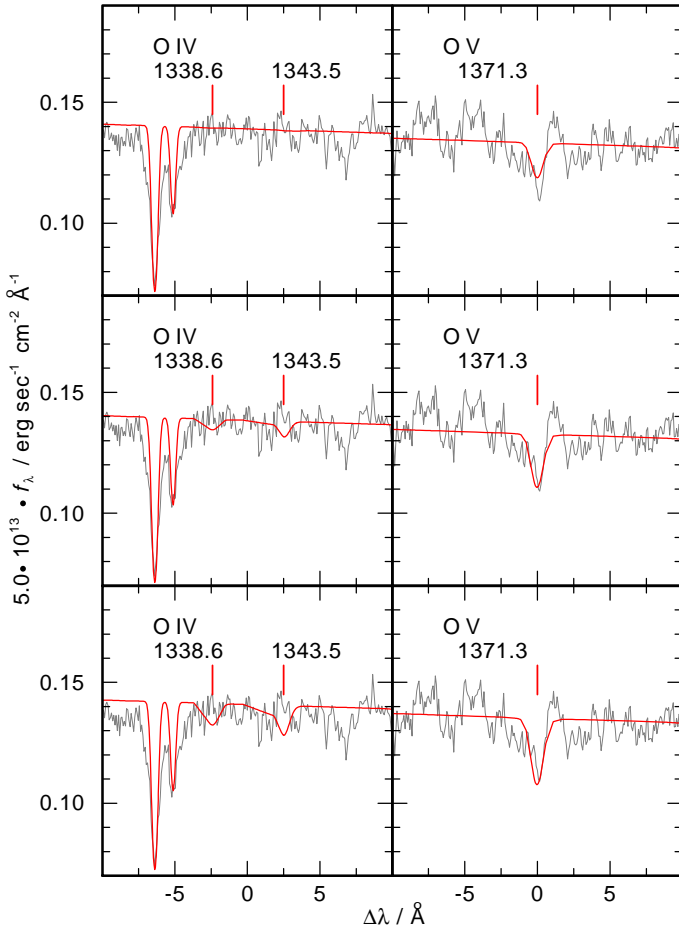
Fig. 18. Determination of T_{eff} of HS 2209+8229 from the O IV / O V ionization equilibrium. Top panels: $T_{eff} = 100\,kK$, middle: $T_{eff} = 110\,kK$; bottom: $T_{eff} = 120\,kK$.
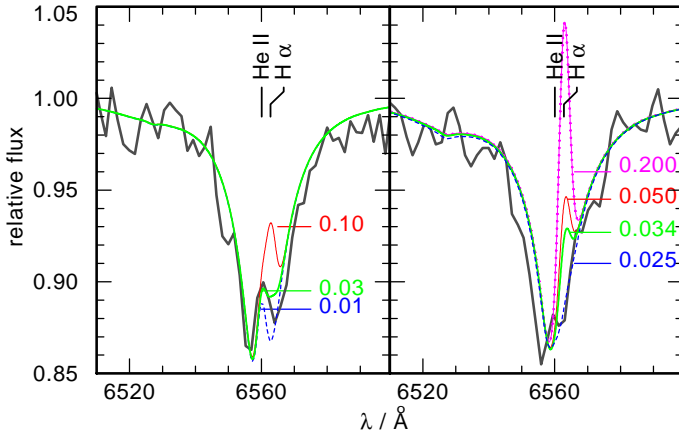

Fig. 19. Determination of the H/He ratio of HS 1522+6615 (left panel) and HS 2209+8229 (right). The observed Hα and He II line blend is compared with models with different H/He mass ratios, as indicated by the labels.

H α is too deep in absorption. For HS 2209+8229, we found that the upper limit of H/He ratio must be lower because of the strong H α emission for H/He > 0.025 (Table 3, Fig. 20).

Carbon The C IV $\lambda\lambda$ 1548.2, 1550.8 Å resonance doublet in the COS spectra of all four stars is contaminated by the respective interstellar lines and therefore unsuited for determining the C

abundance. In the spectra of LoTr 4 and HS 2209+8229 no other C lines were identified and we derived only upper limits of [C][11] < −0.53 and [C] < −1.50, respectively. In the spectrum of K 1−27, we identified C IV $\lambda\lambda$ 1168.8, 1168.9 Å and determined [C] = −0.62. For HS 1522+6615, C IV $\lambda\lambda$ 1168.9, 1169.0 Å in the COS spectrum and C IV $\lambda\lambda$ 5801.33, 5811.98 Å in the optical spectrum were evaluated, and we achieve the best agreement between model and observation at [C] = 0.62. HS 1522+6615 shows the highest, supersolar C abundance (Fig. 21) while the upper limits of the other stars in our sample indicate subsolar abundances.

Nitrogen The N abundance for K 1−27 and LoTr 4 was determined from the N V $\lambda\lambda$ 4603.7, 4619.7, 4933.6, 4943.2, 4945.7 Å emission lines. For HS 2209+8229, we used N V $\lambda\lambda$ 1616.1, 1616.4, 1619.6, 1619.7 Å. As for case of C IV, the resonance doublet N V $\lambda\lambda$ 1238.8, 1242.8 Å is blended by the respective ISM lines. The N abundances of K 1−27 ([N] = 1.28, Fig. 22), LoTr 4 ([N] = 1.07), and HS 2209+8229 ([N] = 2.89) were found to be supersolar, in contrast to the upper limit for HS 1522+6615 ([N] < −0.78), which is subsolar.

Oxygen For K 1−27 and LoTr 4, we derived only upper limits because no O lines except the resonance doublet O VI $\lambda\lambda$ 1031.9, 1037.7 Å were identified, which might be of ISM origin similar to the C IV and N V resonance doublets (Sect. 3.4) We used the O VI $\lambda\lambda$ 1124.7, 1124.8 Å and O VI λ 5290.6 Å to determine the upper limits of [O] < −2.06 for K 1−27 and [O] < −1.47 for LoTr 4. For HS 1522+6615, Rauch et al. (1998) discovered a variability of the O VI λ 5290.6 Å emission feature. Mickaelian et al. (2011) also classified HS 1522+6615 as "possible" variable by comparing the brightness measurements from the Palomar Observatory Sky Survey (POSS) epochs 1 and 2. In view of its variability, we adjusted the O abundance to the co-added optical spectra using O VI $\lambda\lambda$ 3811.4, 3834.2 Å and found [O] = −0.64. A precise determination of the O abundance was possible for HS 2209+8229 using O V λ 1371.3 Å, which is prominent in the COS spectrum (Fig. 23). We found [O] = −1.46 (Table 3).

Fluorine is not identified in the O(He) star spectra. We used F VI λ 1139.5 Å and found [F] < −1.00 for all O(He) stars.

Neon We only derived upper limits using Ne VII $\lambda\lambda$ 1438.8, 1440.5, 1445.0 Å for K 1−27, LoTr 4, and HS 1522+6615 and Ne V $\lambda\lambda$ 1718.2, 1718.3 Å for HS 2209+8229 because of its lower T_{eff}. We determined [Ne] < 0.60 for K 1−27, [Ne] < −0.09 for LoTr 4, [Ne] < −0.62 for HS 1522+6615, and [Ne] < −1.10 for HS 2209+8229.

Silicon An upper limit for the Si abundance was determined using Si IV λ 1128.3 Å, Si V λ 1118.8 Å, and Si VI λ 1130.4 Å. For K 1−27, it is [Si] < −0.56. For LoTr 4, HS 1522+6615, and HS 2209+8229, we derived [Si] < 0.18.

Phosphorus we identified P V $\lambda\lambda$ 1118.0, 1128.0 Å only in the FUSE spectra of LoTr 4 and HS 2209+8229, and we determined

---

[11] [X] denotes log (abundance by mass / solar abundance by mass) of species X. Solar abundances were taken from Asplund et al. (2009).
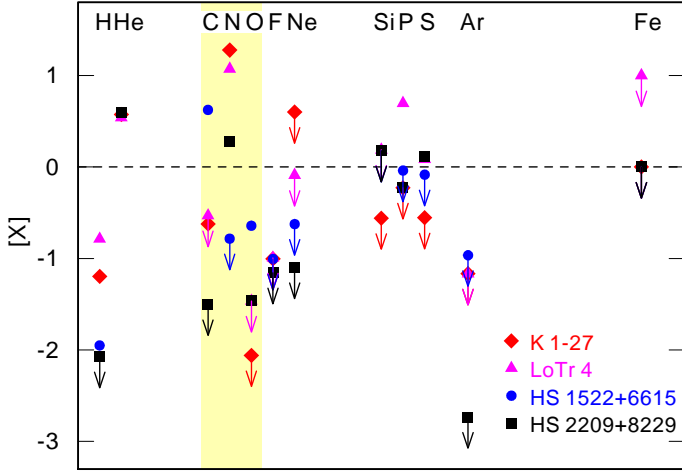
Fig. 20. Abundances of the O(He) stars (Table 3). The shaded (yellow) region emphasizes the CNO differences.

[P] = 0.70 and [P] = −0.76, respectively. For K 1−27 and HS 1522+6615, only upper limits can be given, which are about solar.

Sulfur S VI λ 1117.8 Å was identified in the FUSE spectra of LoTr 4 and HS 2209+8229 and we determined [S] = −0.08 and [S] = −0.11, respectively. For K 1−27 and HS 1522+6615, only upper limits can be given, which are 0.3 times solar and solar, respectively.

Argon is not identified in the O(He) star spectra. We employed Ar VII λ 1535.7, 1537.1, 1537.9 Å and Ar VIII λ 1164.1 Å and derived subsolar upper limits.

Iron The quality of the FUSE spectra is not sufficient to identify individual Fe lines. Therefore, we only included the iron model atom (ionization stages V – IX) in the line-formation calculations (i.e. fixed atmospheric structure) based on our final model and calculated NLTE occupation numbers for the atomic levels of iron. We found that the resulting upper limits of the Fe abundances are solar for K 1−27, HS 1522+6615, and HS 2209+8229. For LoTr 4, we found an upper limit of ten times solar.

3.5. Mass-loss rates

One aim of our COS observations was to follow up on the suggestion of Miller Bertolami & Althaus (2006) that O(He) stars might be post early-AGB stars. The high mass-loss rates invoked in their calculations were not confirmed by our FUSE observations. We performed test calculations based on the final parameters of our analysis (Table 3) using the Potsdam Wolf-Rayet model-atmosphere code, PoWR[12],. This code solves the NLTE radiative transfer in a spherically expanding atmosphere simultaneously with the statistical equilibrium equations and accounts at the same time for energy conservation. Like in TMAP, iron-group line blanking is treated by means of the superlevel approach (Gräfener et al. 2002), and a wind clumping in first-order approximation is taken into account (Hamann & Gräfener

---
[12] http://www.astro.physik.uni-potsdam.de/~wrh/PoWR/

Table 4. Predicted mass-loss rates of the O(He) stars interpolated from Fig. 6a of Pauldrach et al. (1988, P+88) compared with upper limits determined in our analysis (cf. Fig. 25).

object	$\log(\dot{M}/M_\odot$ / yr)	
	P+88	this work
K 1-27	−10.0	≤ −9.0
LoTr 4	−9.4	≤ −9.4
HS 1522+6615	−8.8	≤ −8.8
HS 2209+8229	−10.4	≤ −10.4

2004). We did not calculate hydrodynamically consistent models, but assumed a velocity field following a β-law with $\beta = 1$.

For our calculations, we first used the predicted mass-loss rates ($\dot{M}$) of Pauldrach et al. (1988, Table 4) using the stellar masses determined from comparison with evolutionary tracks of VLTP stars (Fig. 24, Miller Bertolami & Althaus 2006). We considered the terminal wind velocities (v_∞) to be 2.51 times the escape velocities of the stars (Lamers et al. 1995). To then determine an upper limit we increased the mass-loss rate until the synthetic spectra no longer agreed with the observations. We exmained all strategic wind lines that are located in the FUSE and COS wavelength ranges (Fig. 25) and found that only the mass-loss rate of K 1−27, which shows a weak P-Cygni profile at Ne VII λ 973.3 Å in the FUSE spectrum, could be at most an order of magnitude higher than predicted by radiative-driven wind theory. The highest possible $\dot{M}$ values for all O(He) stars are given in Table 4.

4. Stellar parameters and distances

To derive the stellar parameters, we compared the position of the O(He) stars in the log $T_{\rm eff}$ − log g plane with different evolutionary tracks. Fig. 24 shows the location of the O(He) stars and related He-dominated objects compared with an LTP evolutionary track (Miller Bertolami & Althaus 2007) and VLTP post-AGB tracks (Miller Bertolami & Althaus 2006). The LTP and VLTP tracks only differ at low surface gravities, and the masses derived from H-rich post-AGB evolutionary tracks (Miller Bertolami & Althaus 2007) also agree well within the error limits with the VLTP masses. Therefore it is justified to derive the masses of the O(He) stars from these tracks although the VLTP scenario cannot be valid for these stars, as we show below.

We also derived the stellar parameters of the O(He) stars using the evolutionary tracks for double He-WD mergers (Zhang & Jeffery 2012b, Fig. 26). For K 1−27, LoTr 4, and HS 2209+8229, we used the tracks from the slow-merger models because they reproduce the surface abundances of theses stars. For HS 1522+6615 the fast-merger models were used, because they result in C-enriched atmospheres (Sect. 5.2.1). Compared with what we found by comparison with VLTP calculations, luminosities and radii, which were derived from merger processes agree quite well, but the masses are up to $\Delta M = 0.16 M_\odot$ higher (Table 5).

Based on these masses, we calculated the distances (Table 5) by using the flux calibration of Heber et al. (1984) for $\lambda_{\rm eff} = 5454$ Å,

$$d[{\rm pc}] = 7.11 \times 10^4 \cdot \sqrt{H_\nu \cdot M \times 10^{0.4\, m_{v_0} - \log g}},$$

Table 3. Photospheric parameters of the O(He) stars. Our values (R14) are compared with those given by Rauch et al. (1998, R98). Abundances are given as logarithmic mass fraction.

| | K 1−27 | | LoTr 4 | | HS 1522+6615 | | HS 2209+8229 | |
	R14	R98	R14	R98	R14	R98	R14	R98
$T_{\rm eff}$ kK	135^{+5}_{-5}	105^{+10}_{-10}	120^{+10}_{-5}	120^{+12}_{-12}	130^{+10}_{-10}	140^{+14}_{-14}	110^{+10}_{-10}	100^{+10}_{-10}
$\log g$ cm s^{-2}	$6.4^{+0.2}_{-0.3}$	$6.5^{+0.5}_{-0.5}$	$5.8^{+0.2}_{-0.2}$	$5.5^{+0.5}_{-0.5}$	$5.9^{+0.2}_{-0.2}$	$5.5^{+0.5}_{-0.5}$	$6.0^{+0.3}_{-0.3}$	$6.0^{+0.5}_{-0.5}$
H	$-1.33^{+0.41}_{-0.28}$	< -1.30	$-0.92^{+0.21}_{-0.20}$	$-0.90^{+0.30}_{-0.30}$	$-2.08^{+0.47}_{-0.52}$	$-1.60^{+0.30}_{-0.30}$	< -2.21	< -1.30
He	$-0.03^{+0.03}_{-0.03}$	> -0.02	$-0.06^{+0.02}_{-0.05}$	$-0.06^{+0.3}_{-0.3}$	$-0.009^{+0.005}_{-0.009}$	$0.004^{+0.3}_{-0.3}$	> -0.004	> -0.02
C	$-3.25^{+0.45}_{-0.55}$	< -1.82	< -3.14	< -1.92	$-2.00^{+0.68}_{-0.30}$	$-2.05^{+0.3}_{-0.3}$	< -4.13	
N	$-1.88^{+0.36}_{-0.42}$	$-1.76^{+0.3}_{-0.3}$	$-2.10^{+0.60}_{-0.92}$	$-2.45^{+0.3}_{-0.3}$	< -3.94		$-2.89^{+0.89}_{-0.50}$	
O	< -4.30		< -3.73	< -1.50	$-2.88^{+0.60}_{-0.50}$		$-3.00^{+0.70}_{-0.70}$	
F	< -7.30		< -7.29		< -7.30		< -7.45	
Ne	< -2.30		< -2.99		< -3.53		< -4.00	
Si	< -4.06		< -3.00		< -3.00		< -3.00	
P	< -5.52		$-4.54^{+0.40}_{-1.00}$		< -5.20		$-6.00^{+1.00}_{-1.00}$	
S	< -4.07		$-3.43^{+0.61}_{-1.00}$		< -3.59		$-3.40^{+0.88}_{-1.27}$	
Ar	< -5.30		< -4.92		< -5.10		< -6.26	
Fe	< -2.89		< -1.89		< -2.89		< -2.89	

Table 5. Masses $M_{\rm m}$ and $M_{\rm V}$ interpolated from double He-WD mergers (Fig. 26) and evolutionary tracks of VLTP post-AGB stars (Fig. 24), respectively, luminosities L, radii R, Galactic coordinates l and b, distances d, and height above the Galactic plane z of the O(He) stars, as well as the kinematical ages $t_{\rm PN}$ of the two PNe.

	K 1−27	LoTr 4	HS 1522+6615	HS 2209+8829
$M_{\rm m}/M_\odot$	$0.60^{+0.08}_{-0.05}$	$0.70^{+0.08}_{-0.05}$	$0.70^{+0.05}_{-0.05}$	$0.60^{+0.10}_{-0.05}$
$M_{\rm V}/M_\odot$	$0.53^{+0.03}_{-0.01}$	$0.54^{+0.10}_{-0.01}$	$0.57^{+0.07}_{-0.03}$	$0.52^{+0.02}_{-0.01}$
$\log L/L_\odot$	3.2 ± 0.4	3.6 ± 0.3	3.7 ± 0.2	3.2 ± 0.2
$R/R_\odot$	$0.08^{+0.03}_{-0.03}$	$0.14^{+0.05}_{-0.03}$	$0.14^{+0.06}_{-0.02}$	$0.12^{+0.07}_{-0.04}$
$l/°$	286.877	291.434	102.481	117.849
$b/°$	−29.577	+19.258	+44.561	+21.545
$d/$kpc	$2.00^{+0.63}_{-0.84}$	$4.27^{+1.00}_{-1.15}$	$7.86^{+1.72}_{-2.27}$	$2.90^{+0.90}_{-1.24}$
$z/$kpc	$-0.99^{-0.31}_{+0.41}$	$1.41^{+0.33}_{-0.38}$	$5.51^{+1.21}_{-1.59}$	$1.07^{+0.33}_{-0.45}$
$t_{\rm PN}/$yr	10867^{+3421}_{-4553}	16184^{+3794}_{-4360}		

with $m_{\rm V_o} = m_{\rm V} - 2.175c$, $c = 1.47E_{B-V}$, and the Eddington flux H_ν at $\lambda_{\rm eff}$ of our final model atmospheres. All O(He) stars and in particular HS 1522+6615 are located far above or below the Galactic plane (Table 5). K 1−27, LoTr 4, and HS 2209+8829 may belong to the thick disk, which dominates in the region $1\,{\rm kpc} \lesssim z \lesssim 4\,{\rm kpc}$ (Kordopatis et al. 2011). HS 1522+6615 has a high radial velocity of -180 km/s (measured by the shift of e.g. C IV $\lambda\lambda\,1168.9, 1169.0$ Å and He II $\lambda\,1640.4$ Å in the COS spectrum). Using the proper motions from the Sloan Digital Sky Survey Photometric Catalog (Release 9, Ahn et al. 2012), we calculated the space velocities to $U = 95$ km/s, $V = -116$ km/s, and $W = -121$ km/s, which are typical for halo stars (Kordopatis et al. 2011). From large height above the Galactic

plane ($z = 5.51$ kpc) of HS 1522+6615 and its fast space velocities, we conclude that it belongs to the Galactic halo.

Using a typical expansion velocity of 20 km/s for the PNe of K 1−27 and LoTr 4, we also calculated their kinematical ages. The results are given in Table 5.

5. Results and discussion

We re-analyzed all known O(He) stars based on the available spectra and improved the determination of their properties (Tables 3, 5). We found that C, N, O, and Ne have a strong impact on the atmospheric structure and thus a strong effect on the resulting line profiles. This mostly affected K 1−27, for which we found a 30 kK higher $T_{\rm eff}$ than in literature. The COS observations allowed us to determine the N and O abundances for HS 2209+8229 for the first time. The FUSE observation of K 1−27 allowed us to determine the C abundances for this star for the first time. We derived upper abundance limits for F, Ne, Si, P, S (for LoTr 4 and HS 2209+8229 the actual abundance values for P and S, measured from the FUSE spectrum), Ar, and Fe.

By examining all strategic wind-lines located in the FUSE and COS wavelength ranges, we found that the upper limits for mass-loss rates of the O(He) stars agree well with predictions by radiative-driven wind theory. Only K 1−27 might have a ten times higher mass-loss rate than predicted (only there did we find spectral signatures). From comparison with stellar-evolution calculations we found that the masses of the O(He) stars range from $0.52\,M_\odot$ to $0.57\,M_\odot$ considering (V)LTP tracks, or from $0.60\,M_\odot$ to $0.70\,M_\odot$ considering double He-WD merger tracks.

Before considering possible evolutionary scenarios, it is worth to mention, that the CNO abundance patterns are similar for all O(He) stars exept HS 1522+6615 (Fig. 20), which exhibits strongly deviating CNO abundances. This suggests a di-
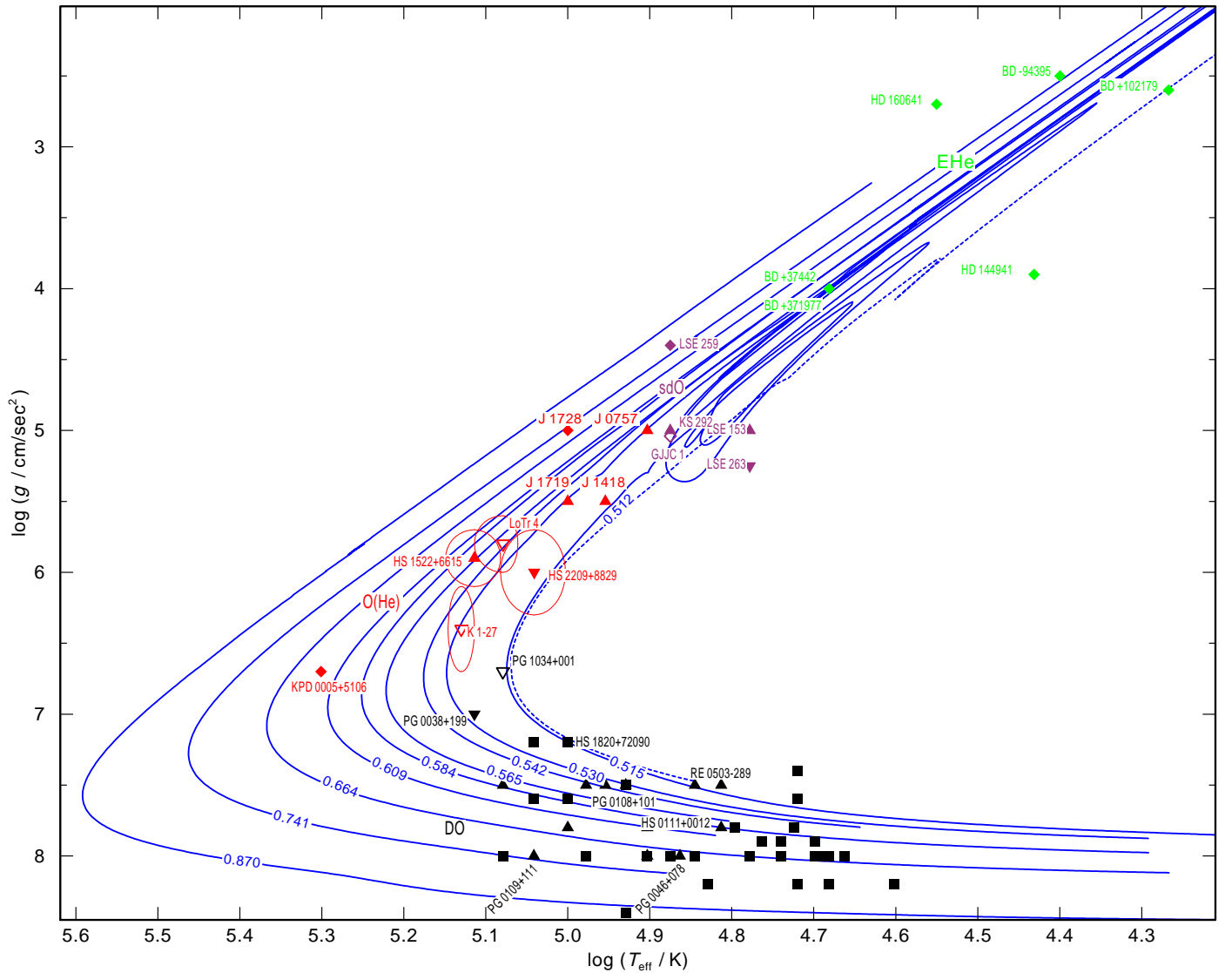
Fig. 24. Locations of EHe stars (green, Jeffery & Hamann 2010) the luminous sdO-stars (purple, Müller-Ringat 2013; Rauch et al. 1998, 1991; Husfeld et al. 1989) and O(He) stars (red, this work, Werner et al. 2014; Wassermann et al. 2010) as well as the DO WDs (black, Werner et al. 2014; Mahsereci 2011; Hügelmeyer et al. 2006; Dreizler & Werner 1996) in the $\log T_{\mathrm{eff}} - \log g$ plane compared with an LTP (dashed line) and VLTP post-AGB (solid lines) evolutionary tracks (labeled with stellar masses in $M_{\odot}$) of Miller Bertolami & Althaus (2006). Open symbols indicate CSPNe, filled ones indicate that no PN was detected. C-rich objects are represented by triangles, N-rich objects by inverted triangles, C- and N-rich objects by diamonds. Squares specify objects that are neither enriched in C nor in N.

chotomy within the O(He) class. Interestingly, we find that other He-dominated objects (e.g. He-rich subdwarfs; Müller-Ringat 2013; Németh et al. 2012; Naslim et al. 2010; Hirsch 2009; Ahmad et al. 2004; Rauch et al. 1998, 1991; Husfeld et al. 1989; Stroeer et al. 2007, DO WDs Werner et al. 2014; Mahsereci 2011; Hügelmeyer et al. 2006; Dreizler & Werner 1996) also show these differences in the CNO abundances[13].

Some objects which are enriched in N but not in C, some C-enriched objects do not show N, but there also are objects which are enriched in both. This suggests that there exist subclasses within the He-dominated objects. Each of them might have a different evolutionary history. From the He-dominated post-AGB objects (Fig. 24), it seems that there is no correlation of the stellar mass and the C-enriched objects. There is no star

among N-enriched objects with a higher mass than $0.542 M_{\odot}$. This might be because for low-mass stars no third drege-up is predicted during the AGB evolution (Mello et al. 2012). The C- and N-enriched sdO and O(He) stars have masses greater than $0.64 M_{\odot}$.

Rauch et al. (1998) already proposed the
$$\mathrm{sdO(He)} \rightarrow \mathrm{O(He)} \rightarrow \mathrm{DO\ WD}$$
evolutionary channel that runs parallel to the PG 1159 evolution in the HRD. However, they were unable to present stringent clues on the evolution of O(He) stars. In the following we discuss different evolutionary channels to explain the origin of the O(He) stars, but also investigate the origin of other He-dominated objects to find possible progenitors and successors. First we will mention single-star evolutionary channels (Sect. 5.1), such as enhanced mass-loss of post early-AGB stars, (V)LTP scenarios, and the hot-flasher scenario. In Sect. 5.2 we consider to formation channels in binary systems, starting with

---

[13] A list of all analyzed He-rich sdO stars, that are enriched in N and/or C, O(He) stars and DO WDs can be found at http://astro.uni-tuebingen.de/~reindl/He .
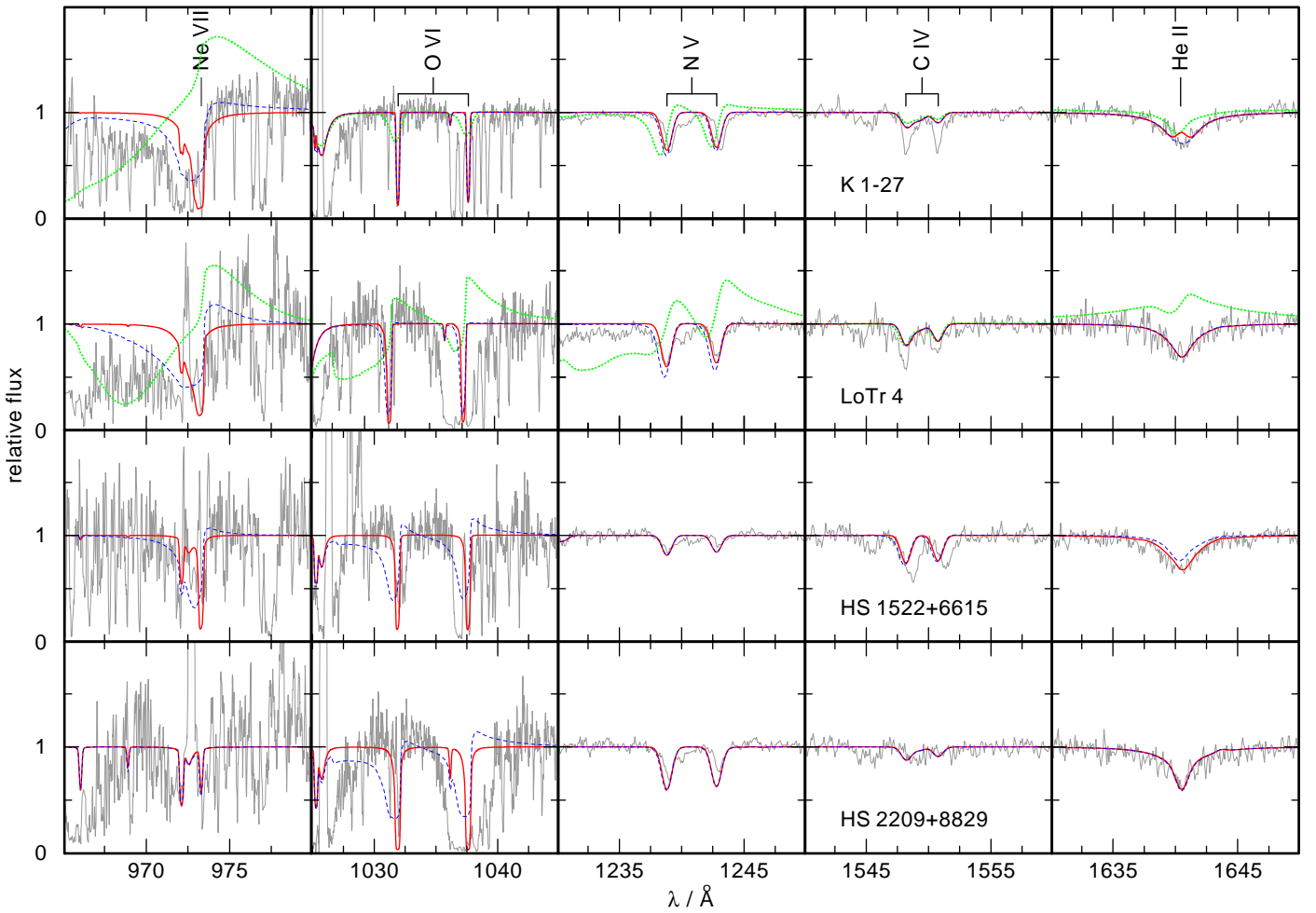
Fig. 25. Synthetic PoWR line profiles of Ne VII 2p ^{1}P^o − 2p ^{1}D, of the resonance doublets of O VI, N V, C IV, and of He II λ 1640 Å calculated with mass-loss rates from Pauldrach et al. (1988, red lines) and 10 × and 100 × (K 1−27 and LoTr 4 only) enhanced mass-loss rates (blue, dashed and green, dotted lines, respectively), compared with the observations of the four O(He) stars.

the merger scenarios (Sect. 5.2.1). We also discuss problems of this formation channel and some other possible binary formation channels such as enhanced mass-loss triggered by a planet or brown dwarf and the merger of a He and CO WD (Sect. 5.2.2).

5.1. Single-star evolution

Assuming single-star evolution, Rauch et al. (2009) suggested that low-mass O(He) stars might be post early-AGB stars that experienced an enhanced mass-loss which removed the H-rich envelope. In these stars, the first thermal pulse occurs after their departure from the AGB. A numerical experiment for a $0.512\,M_\odot$ star by Miller Bertolami & Althaus (2006) has shown that an artificially increased mass-loss rate can cause the hydrogen deficiency and, in the later evolution, might turn the O(He) stars into PG 1159 stars. However, to achieve that Miller Bertolami & Althaus (2006) had to assume $\log \dot{M}/(M_\odot\,/\,\mathrm{yr}) = -8$ for $\log T_{\mathrm{eff}} > 3.8$. Such a strong wind is not predicted by radiative-driven wind theory nor is it seen in the spectra of the O(He) stars. Only K 1−27 could have a ten times higher mass-loss rate than predicted, but the derived upper limited ($\log \dot{M}/(M_\odot\,/\,\mathrm{yr}) = -9$) is still too low to overcome the He-buffer and consequently turn the O(He) star into a PG 1159 star. The previous mass-loss history of the O(He) stars is of course unknown and we can therefore only rule out PG 1159 stars as

possible successors of O(He) stars. However, the different H-abundances of the N-enriched O(He) stars, show a correlation with stellar mass and hence the post-AGB times and the remaining H in the atmospheres of these stars. While LoTr 4 still shows 12 % H (by mass), the more evolved and lower mass K 1−27 only shows 5 % H. No H can be detected in the spectrum in the lowest mass O(He) star, HS 2209+8229. Although the predicted mass-loss rates are lower for stars with lower mass, their evolutionary timescales are much longer, and that is why the correlation of stellar mass and remaining H seems plausible if enhanced mass-loss is assumed.

Within this scenario, good candidates for successors are C-enriched DO WDs (e.g. PG 0108+101, HS 0111+0012, Dreizler & Werner 1996) for HS 1522+6615 or N-enriched DO WDs (e.g. PG 0038+199, PG 1034+001, Mahsereci 2011) for the three other O(He) stars. However, because of gravitational settling they might also turn into DOs, which do not show any C or N anymore, or even, depending on the remaining H, into DA WDs.

Possible progenitors might be luminous helium-rich sdO-type stars, for example LSE 153 (Müller-Ringat 2013) for HS 1522+6615 or LSE 263 (Müller-Ringat 2013) for the N-enriched O(He) stars.

Other interesting objects that fit into this sequence, might be the [WN]-type CSPNe IC 4663 (Miszalski et al. 2012) and
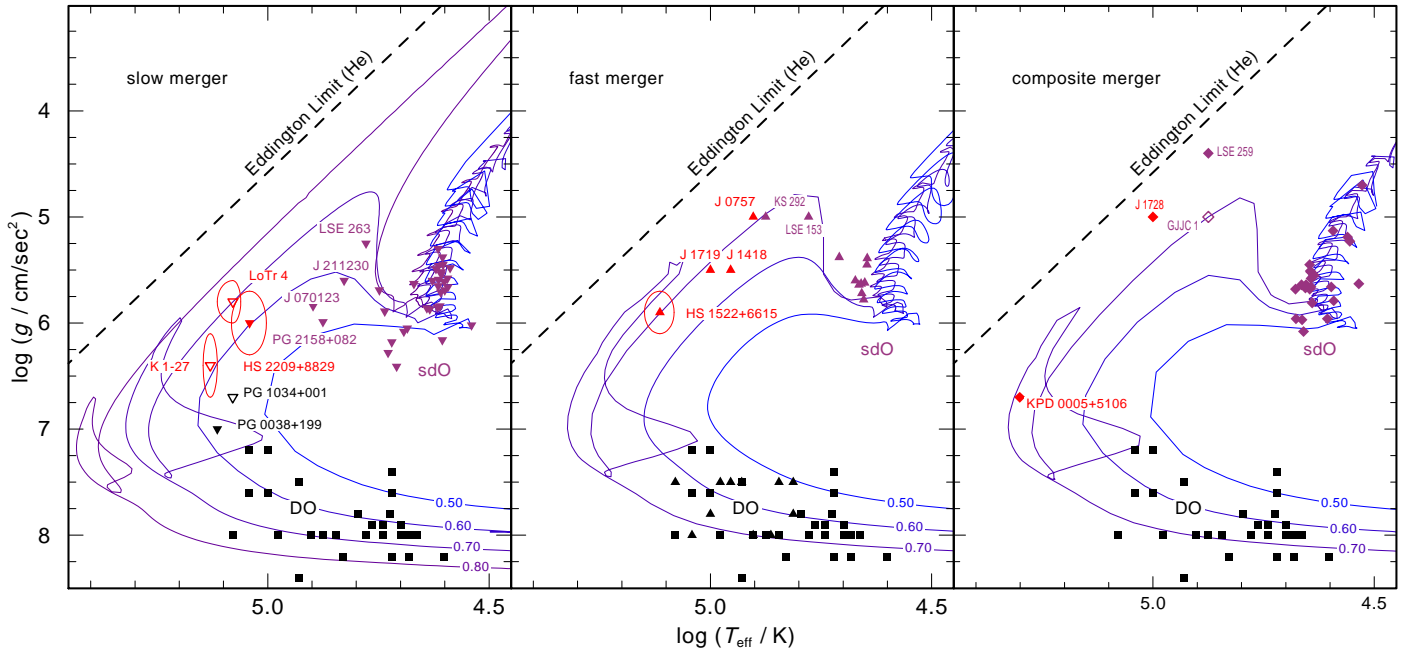
Fig. 26. Evolutionary tracks for a slow-merger (left), a fast-merger (middle) and a composite-merger (right) scenario of two He-WDs, marked with the merger mass in $M_\odot$ (Zhang & Jeffery 2012b). The locations of the sdB-, sdO-stars, (purple, Müller-Ringat 2013; Németh et al. 2012; Naslim et al. 2010; Hirsch 2009; Ahmad et al. 2004; Rauch et al. 1998, 1991; Husfeld et al. 1989; Stroeer et al. 2007) and O(He) stars (red this work, Werner et al. 2014; Wassermann et al. 2010) as well as the DO WDs (black, Werner et al. 2014; Mahsereci 2011; Hügelmeyer et al. 2006; Dreizler & Werner 1996) are marked. Open symbols indicate CSPNe, filled ones that no PN was detected. C-rich objects are represented by triangles, N-rich objects by inverted triangles, C- and N-rich objects by diamonds. Squares specify objects that are neither enriched in C nor in N.

Abell 48 (Todt et al. 2013; Frew et al. 2014). Because of the strong similarity of the element abundances of [WN] stars and the N-enriched O(He) stars, an analog to the H-deficient, but C-rich post-AGB sequence [WCL] → [WCE] → PG 1159 (e.g. Werner & Herwig 2006), a second, H-deficient sequence [WN] → O(He) was suggested (cf. Werner 2012). By examining He II λ 4686 Å and Ne VII λ 3890 Å, Miszalski et al. (2012) determined $T_{\rm eff} = 140$ kK for IC 4663. Their values for the mass and the surface gravity ($M = 0.6\,M_\odot$ and $\log g = 6.1$) are only estimates, however. With $T_{\rm eff} = 140$ kK, IC 4663 would be in a similar or even later evolutionary state than the O(He) stars. Abell 48 ($T_{\rm eff} = 70$ kK), on the other hand, is in an earlier evolutionary stage than the O(He) stars. Still, it is necessary to clarify why IC 4663 and Abell 48 show a much stronger stellar wind (IC 4663: $\log \dot{M}/M_\odot/{\rm yr} = -7.7$, Abell 48: $\log \dot{M}/M_\odot/{\rm yr} = -6.4$) than the O(He) stars. We speculate that [WN] stars are O(He) stars with higher masses. According to Pauldrach et al. (1988, Fig. 6b), the high mass-loss rate found for IC 4663 and Abell 48 would correspond to $M \approx 0.7\,M_\odot$ and $M > 1.0\,M_\odot$, respectively.

Rauch et al. (2008) suggested that RCB stars might be possible progenitors of the O(He) stars. This could be true for the two C and N enriched O(He) stars SDSS J 172854.34+361958.62 (Werner et al. 2014) and KPD 0005+5106 (Wassermann et al. 2010). In between evolutionary objects could be the C- and N-enriched luminous sdO stars LSE 259 (Husfeld et al. 1989), GJJC 1 (Rauch et al. 1998), and KS 292 (Rauch et al. 1991).

The VLTP scenarios that were successfully applied to explain the origin of the H-deficient, but C-rich objects (e.g. PG 1159 stars) cannot explain the origin of the O(He) stars because these scenarios always produce C-rich atmospheres with more than about 20 % of C by mass (in contrast, the most C-rich O(He) stars only show 3% of C in their atmospheres). The relatively young kinematical age of the H-rich PNe of

K 1−27 and LoTr 4 (around 10 000 yrs) strongly contradict a VLTP scenario.

A third conceivable way for a single-star evolutionary channel is the hot-flasher scenario, which was invoked by Miller Bertolami et al. (2008) to explain the helium-rich sdO stars. This scenario is able to explain C- or N-enriched He-sdOs, but these stellar models never reach the high effective temperatures found for the O(He) stars.

5.2. Binary evolution

Since none of the previously mentioned single-star formation channels seems convincing for the O(He) stars, binary formation channels become interesting. We discuss merger scenarios and suggest alternatives.

5.2.1. Merger scenarios

As mentioned above, Zhang & Jeffery (2012b,a) showed that in terms of $T_{\rm eff}$, $\log g$, C, and N abundances, the origin of the three sdOs groups, but also the properties of RCB and EHe stars, can be explained by different double He-WD merger models. Zhang & Jeffery (2012a) compared their result with He-rich sdO stars from the sample of Hirsch (2009) and He-rich sdB stars from the sample Naslim et al. (2010). We extended this comparison to all He-rich sdB and sdO stars, that are enriched in C and/or N (Müller-Ringat 2013; Németh et al. 2012; Naslim et al. 2010; Hirsch 2009; Ahmad et al. 2004; Rauch et al. 1998, 1991; Husfeld et al. 1989; Stroeer et al. 2007), the O(He) of our work, and those of Werner et al. (2014); Wassermann et al. (2010), and the known DO WDs (Werner et al. 2014; Mahsereci 2011; Hügelmeyer et al. 2006; Dreizler & Werner 1996). We found that all of them fit this scenario. Figure 27 shows the

CNO abundances resulting from a slow and a fast merger of two He WDs according to the numerical experiments of Zhang & Jeffery (2012a). These abundances are compared with those of the O(He) stars analyzed in our work. We found that those of the two CSPNe and HS 2209+8229 can be explained by the slow-merger model and the CNO abundances of HS 1522+6615 are reproduced by the fast-merger because of the high C abundance. The three O(He) stars SDSS J 171916.97+365326.70, SDSS J 141812.50+024426.92, and SDSS J 075732.18+184329.28 that were found by Werner et al. (2014) also fit the fast-merger scenario. SDSS J 172854.34+361958.62 (Werner et al. 2014) and KPD 0005+5106 (Wassermann et al. 2010) would fit the composite merger model. Concerning the CNO abundances, the O(He) stars can be explained much better by this double He WD merger scenario than by V(LTP) scenarios. Fig. 26 shows the evolutionary tracks of Zhang & Jeffery (2012a) for their different merger models. Following to their surface abundances, which are produced in a certain merger model, we marked the locations of the N-enriched He-dominated objects in the panel for the slow merger, C-enriched ones in the fast-merger panel, and C- and N-enriched objects are shown in the composite merger panel. These evolutionary tracks connect the subluminous sdO with the luminous sdO stars (in contrast to the VLTP calculations), the O(He) stars, and DO WDs.

Other points that support the merger scenario are the very low binary fraction among He-rich sdO-stars (4%, Napiwotzki et al. 2004), O(He) stars, and DO WDs (only PG 0046+078 and PG 0237+116 have been found to be in a binary system). A different development scenario probably applies for binary systems. The position of HS 1522+6615 in the Galactic halo corroborates the merger scenario, because only very old stars are expected there. Napiwotzki (2008) found that a considerable part (20%) of the He-rich sdO stars belongs to the halo population. The fact that no PN is detected around HS 1522+6615, SDSS J 171916.97+365326.70, SDSS J 141812.50+024426.92, and SDSS J 075732.18+184329.28 although their theoretical post-AGB evolutionary times would be shorter than those of K 1−27 or LoTr 4, might be explained considering that these objects are merger products.

We note that the WD+post-sdB star merger channel, proposed by Justham et al. (2011) to explain He-rich sdO stars, can explain the O(He) stars in terms of $T_{\rm eff}$ and $\log g$ as well.

5.2.2. Alternative scenarios

Within the merger models mentioned above it is not possible to explain the PNe of K 1−27 and LoTr 4. Even if a PN would have been ejected during the merger process, it would have dissipated into the ISM a long time ago because the post-merger time of LoTr 4 is about $3.7 \cdot 10^7$ years. In addition, the solar compositions of the PNe of K 1−27 and LoTr 4 and the remaining hydrogen in their atmospheres contradicts a merger origin of these objects. The same holds for GJJC 1, IC 4663 and PG 1034+001. For these reasons *common envelope (CE) scenarios* become interesting. Soker (2013) speculated that R CrB itself and similar RCB stars are formed from the merger of a WD with the core of an AGB star. The previous common-envelope ejection (CEE) then would have caused the H-deficiency. This scenario would also be possible for the O(He) stars. The merger within a CE of a CO-WD and a RG or AGB star might produce a similar outcome as a *He- and CO-WD merger* but *within a H-rich envelope*. The CE ejected
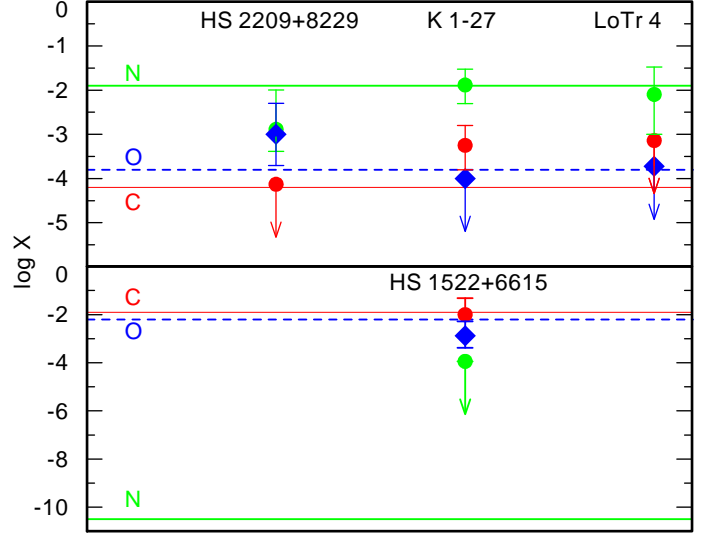

Fig. 27. Comparison of the CNO abundances of the O(He) stars (N: light, green dots, C: dark, red dots, O: dark, blue rhombi, with those resulting form a slow (top) and a fast (0.7 $M_\odot$ model, bottom) merger of two He WDs (N: light, green, solid line, C: dark, red, solid line, O: dashed, blue, gray line).

during the merger process could then first reproduce the H-rich PNe of K 1−27 and LoTr 4 and then, the post-merger times would be much shorter because no central helium burning phase is expected for a He- and CO-WD merger.

Another possibility for a O(He) star origin is that an *RG or AGB star lost its H-rich envelope with the help of a planet or a brown dwarf*. If a low-mass companion enters the atmosphere of an RG or AGB star, it spirals inwards and transfers orbital energy and angular momentum to the envelope and, thus, parts or all of it are removed. The companion then either stops in a close orbit or even merges with the more massive star (Diehl et al. 2008; Soker 1998).

5.3. Conclusions

The evolutionary status of the O(He) stars, but also those of other He-dominated stars, is still not understood. It is most likely that they are part of a second H-deficient evolutionary sequence. It appears plausible that there are three subclasses within this He-dominated sequence. For objects that are either enriched in C or N, we propose the channels

sdO(He) → O(He) → DO WD

or

sdO(He) → O(He) → DA WD

if there is some remaining H. For C- and N-rich objects, we propose

RCB → EHe → sdO(He) → O(He) → DO WD

or

RCB → EHe → sdO(He) → O(He) → DA WD

if that there is some remaining H.

This He-dominated sequence has most likely various formation channels. For single-star objects, merger scenarios seem most promising. He-dominated CSPNe, must have formed in a different way, for example via enhanced mass-loss during their post-AGB evolution or a merger within a CE of a CO-WD and an RG or AGB star.

To make progress, it would be highly desirable that more O(He) stars and other He-dominated objects were discovered to improve the statistics. Additional quantitative investigations on the binarity of these objects and on the mass-loss rates of RCB, EHe, and sdO stars may help to distinguish between different formation channels. A comprehensive systematic calculation of evolutionary models for thermal pulse and merger scenarios is a pre-requisite for comparision with results of spectral analysis.

References

Ahmad, A., Jeffery, C. S., & Fullerton, A. W. 2004, A&A, 418, 275

Ahn, C. P., Alexandroff, R., Allende Prieto, C., et al. 2012, ApJS, 203, 21

Asplund, M., Grevesse, N., Sauval, A. J., & Scott, P. 2009, ARA&A, 47, 481

Bucciarelli, B., García Yus, J., Casalegno, R., et al. 2001, A&A, 368, 335

Clayton, G. C., Sugerman, B. E. K., Stanford, S. A., et al. 2011, ApJ, 743, 44

Diehl, S., Fryer, C., & Herwig, F. 2008, in Astronomical Society of the Pacific Conference Series, Vol. 391, Hydrogen-Deficient Stars, ed. K. Werner & T. Rauch, 221

Dreizler, S. & Werner, K. 1994, in Evolution of Massive Stars, ed. D. Vanbeveren, W. van Rensbergen, & C. De Loore, 147

Dreizler, S. & Werner, K. 1996, A&A, 314, 217

Fitzpatrick, E. L. 1999, PASP, 111, 63

Frew, D. J., Bojičić, I. S., Parker, Q. A., et al. 2014, MNRAS, 440, 1345

Gräfener, G., Koesterke, L., & Hamann, W.-R. 2002, A&A, 387, 244

Hamann, W.-R. & Gräfener, G. 2004, A&A, 427, 697

Han, Z., Podsiadlowski, P., Maxted, P. F. L., & Marsh, T. R. 2003, MNRAS, 341, 669

Han, Z., Podsiadlowski, P., Maxted, P. F. L., Marsh, T. R., & Ivanova, N. 2002, MNRAS, 336, 449

Heber, U., Hunger, K., Jonas, G., & Kudritzki, R. P. 1984, A&A, 130, 119

Hébrard, G., Lemoine, M., Vidal-Madjar, A., et al. 2002, ApJS, 140, 103

Hébrard, G. & Moos, H. W. 2003, ApJ, 599, 297

Hirsch, H. A. 2009, PhD thesis, University Nuremberg

Hügelmeyer, S. D., Dreizler, S., Homeier, D., et al. 2006, A&A, 454, 617

Husfeld, D., Butler, K., Heber, U., & Drilling, J. S. 1989, A&A, 222, 150

Jeffery, C. S. & Hamann, W.-R. 2010, MNRAS, 404, 1698

Jeffery, C. S., Karakas, A. I., & Saio, H. 2011, MNRAS, 414, 3599

Justham, S., Podsiadlowski, P., & Han, Z. 2011, MNRAS, 410, 984

Kameswara Rao, N., Lambert, D. L., García-Hernández, D. A., & Manchado, A. 2013, MNRAS, 431, 159

Kordopatis, G., Recio-Blanco, A., de Laverny, P., et al. 2011, A&A, 535, A107

Lamers, H. J. G. L. M., Snow, T. P., & Lindholm, D. M. 1995, ApJ, 455, 269

Mahsereci, M. 2011, Diploma thesis, University Tübingen

Mello, D. R. C., Daflon, S., Pereira, C. B., & Hubeny, I. 2012, A&A, 543, A11

Méndez, R. H., Miguel, C. H., Heber, U., & Kudritzki, R. P. 1986, in Astrophysics and Space Science Library, Vol. 128, IAU Colloq. 87: Hydrogen Deficient Stars and Related Objects, ed. K. Hunger, D. Schönberner, & N. Kameswara Rao, 323

Mickaelian, A. M., Mikayelyan, G. A., & Sinamyan, P. K. 2011, MNRAS, 415, 1061

Miller Bertolami, M. M. & Althaus, L. G. 2006, A&A, 454, 845

Miller Bertolami, M. M. & Althaus, L. G. 2007, A&A, 470, 675

Miller Bertolami, M. M., Althaus, L. G., Unglaub, K., & Weiss, A. 2008, A&A, 491, 253

Miszalski, B., Crowther, P. A., De Marco, O., et al. 2012, MNRAS, 423, 934

Müller-Ringat, E. 2013, Dissertation, University of Tübingen, Germany, http://tobias-lib.uni-tuebingen.de/volltexte/2013/6774/

Napiwotzki, R. 2008, in Astronomical Society of the Pacific Conference Series, Vol. 391, Hydrogen-Deficient Stars, ed. K. Werner & T. Rauch, 257

Napiwotzki, R., Karl, C. A., Lisker, T., et al. 2004, Ap&SS, 291, 321

Naslim, N., Jeffery, C. S., Ahmad, A., Behara, N. T., & Şahìn, T. 2010, MNRAS, 409, 582

Németh, P., Kawka, A., & Vennes, S. 2012, MNRAS, 427, 2180

Pauldrach, A., Puls, J., Kudritzki, R. P., Méndez, R. H., & Heap, S. R. 1988, A&A, 207, 123

Rauch, T. & Deetjen, J. L. 2003, in Astronomical Society of the Pacific Conference Series, Vol. 288, Stellar Atmosphere Modeling, ed. I. Hubeny, D. Mihalas, & K. Werner, 103

Rauch, T., Dreizler, S., & Wolff, B. 1998, A&A, 338, 651

Rauch, T., Heber, U., Hunger, K., Werner, K., & Neckel, T. 1991, A&A, 241, 457

Rauch, T., Köppen, J., & Werner, K. 1994, A&A, 286, 543

Rauch, T., Köppen, J., & Werner, K. 1996, A&A, 310, 613

Rauch, T., Reiff, E., Werner, K., et al. 2006, in Astronomical Society of the Pacific Conference Series, Vol. 348, Astrophysics in the Far Ultraviolet: Five Years of Discovery with FUSE, ed. G. Sonneborn, H. W. Moos, & B.-G. Andersson, 194

Rauch, T., Reiff, E., Werner, K., & Kruk, J. W. 2008, in Astronomical Society of the Pacific Conference Series, Vol. 391, Hydrogen-Deficient Stars, ed. K. Werner & T. Rauch, 135

Rauch, T., Werner, K., & Kruk, J. W. 2009, in American Institute of Physics Conference Series, Vol. 1135, American Institute of Physics Conference Series, ed. M. E. van Steenberg, G. Sonneborn, H. W. Moos, & W. P. Blair, 168

Savitzky, A. & Golay, M. J. E. 1964, Analytical Chemistry, 36, 1627

Soker, N. 1998, AJ, 116, 1308

Soker, N. 2013, New A, 18, 18

Stroeer, A., Heber, U., Lisker, T., et al. 2007, A&A, 462, 269

Todt, H., Kniazev, A. Y., Gvaramadze, V. V., et al. 2013, MNRAS, 430, 2302

Wassermann, D., Werner, K., Rauch, T., & Kruk, J. W. 2010, A&A, 524, A9

Werner, K. 2012, in IAU Symposium, Vol. 283, Planetary Nebulae: An Eye to the Future, 196

Werner, K., Deetjen, J. L., Dreizler, S., et al. 2003, in Astronomical Society of the Pacific Conference Series, Vol. 288, Stellar Atmosphere Modeling, ed. I. Hubeny, D. Mihalas, & K. Werner, 31

Werner, K. & Herwig, F. 2006, PASP, 118, 183

Werner, K., Rauch, T., & Kepler, S. O. 2014, A&A, 564, A53

Zhang, X. & Jeffery, C. S. 2012a, MNRAS, 426, L81
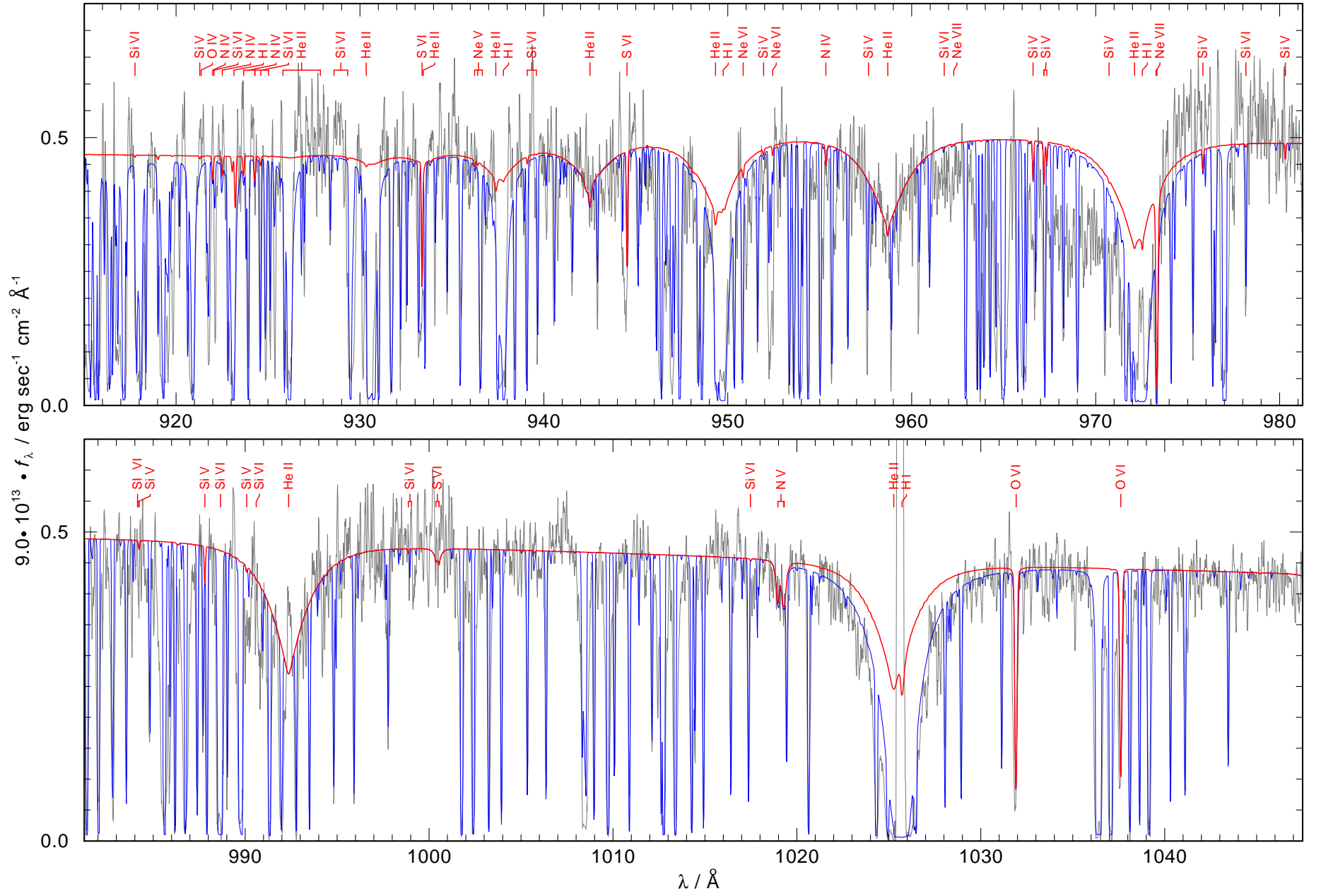
Zhang, X. & Jeffery, C. S. 2012b, MNRAS, 419, 452

Fig. 1. FUSE spectrum of K 1−27 (gray) compared with final synthetic spectra (red: pure stellar, blue: combined stellar and interstellar). The locations of photospheric lines appearing in the synthetic spectrum are marked.
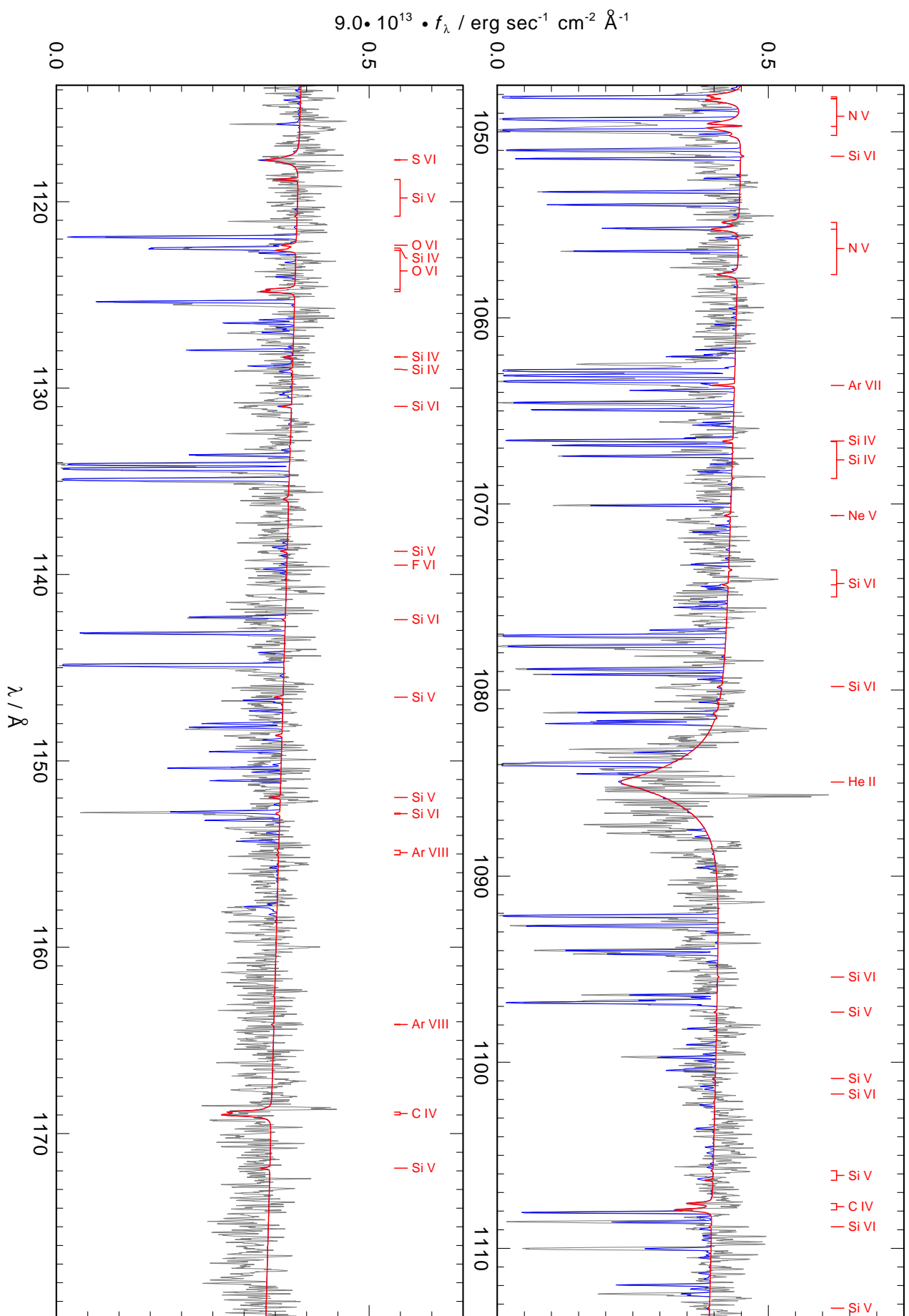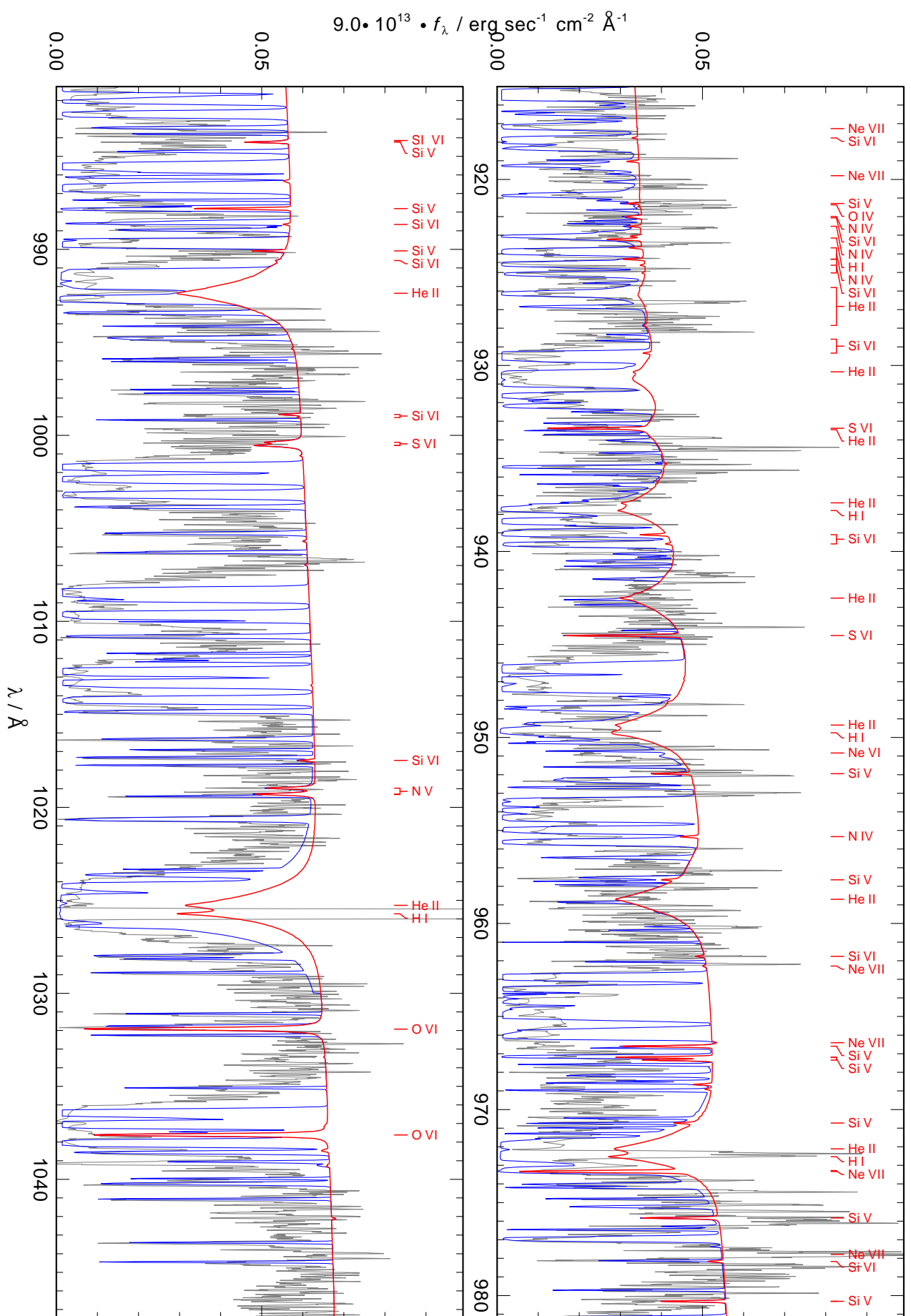
Fig. 1. Continued.

A&A–AA_ohe, Online Material p 14
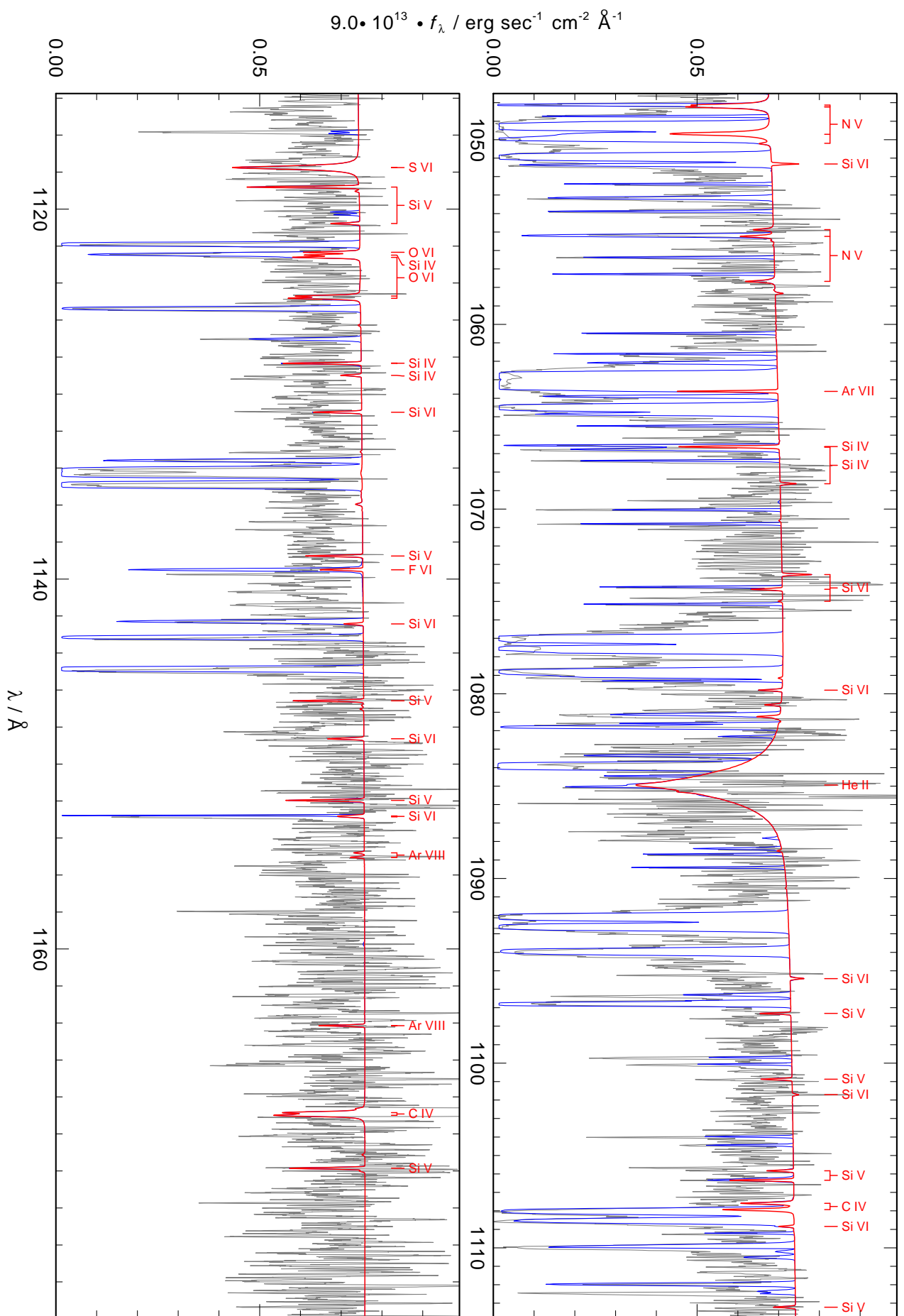
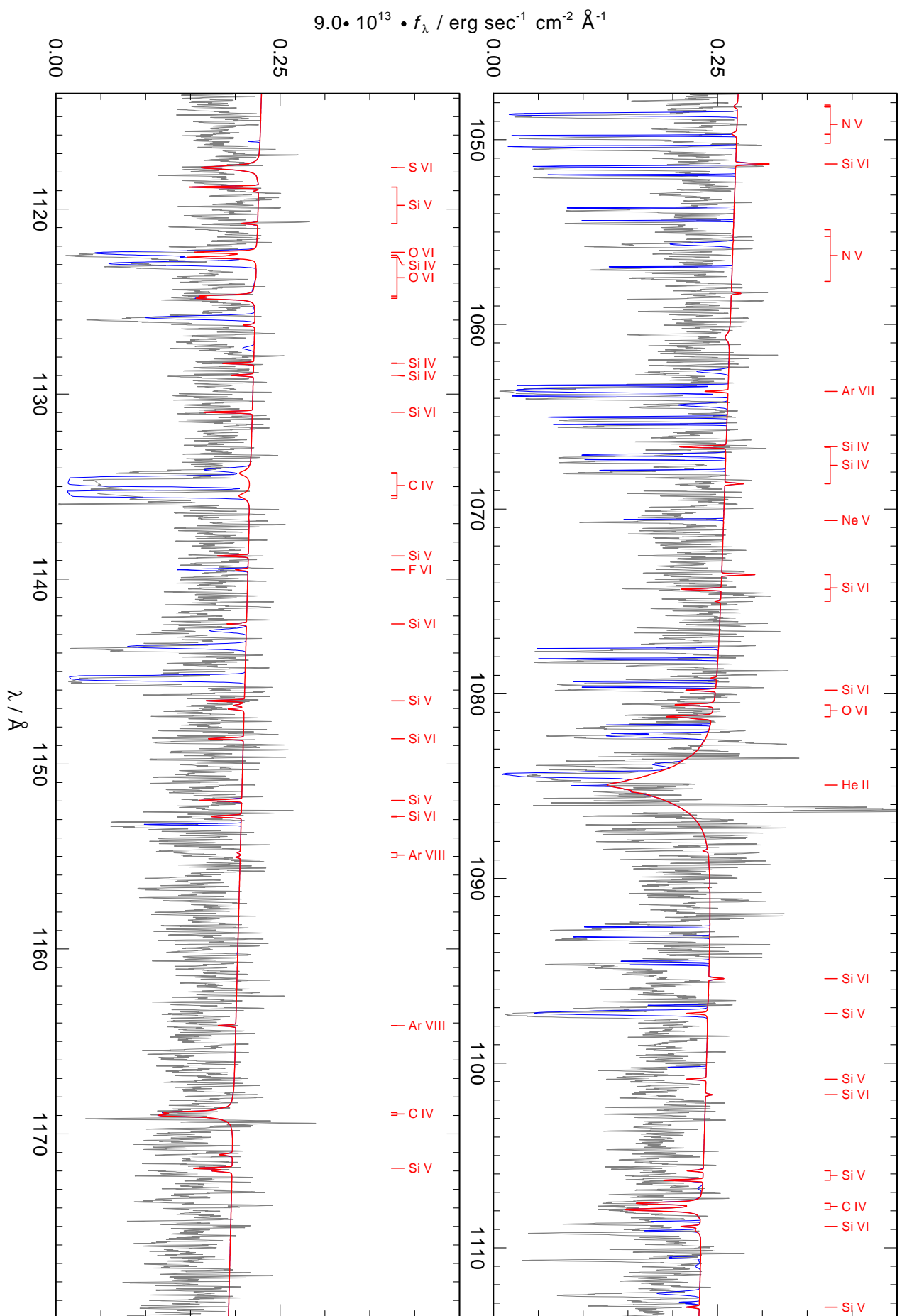**Fig. 2.** Same as Fig. 1 for LoTr 4.

Fig. 2. Continued.
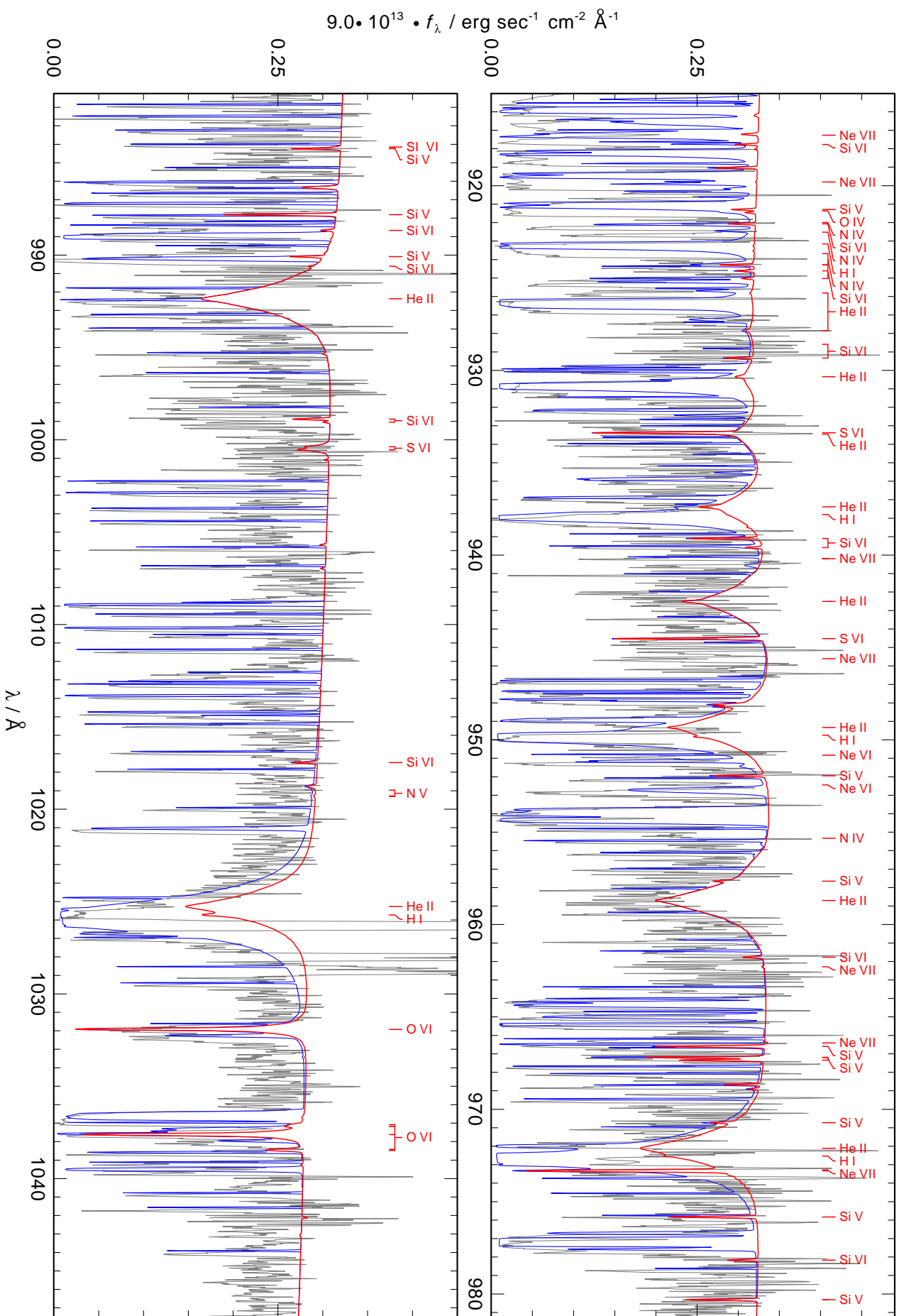
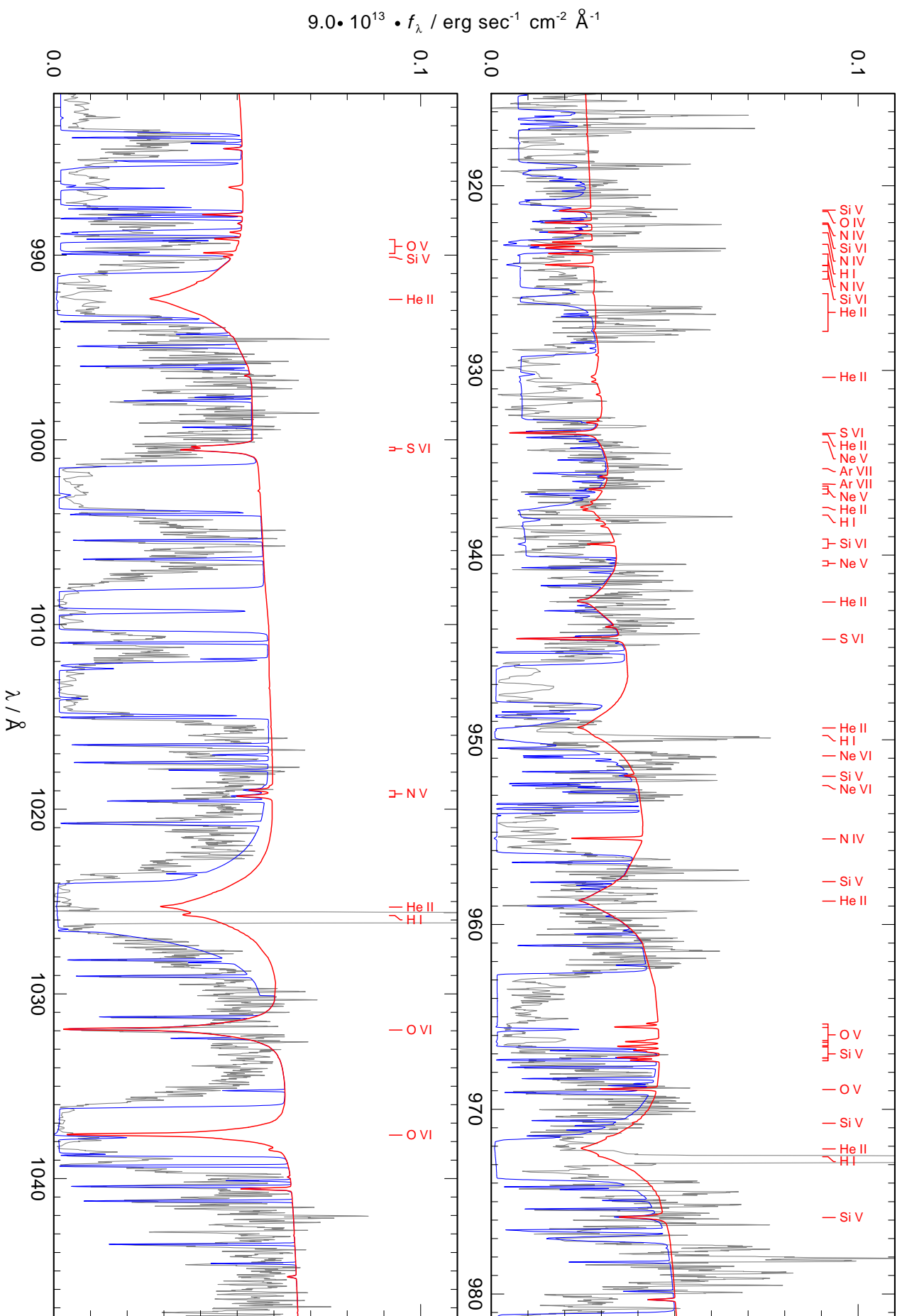**Fig. 3.** Same as Fig. 1 for HS 1522+6615.

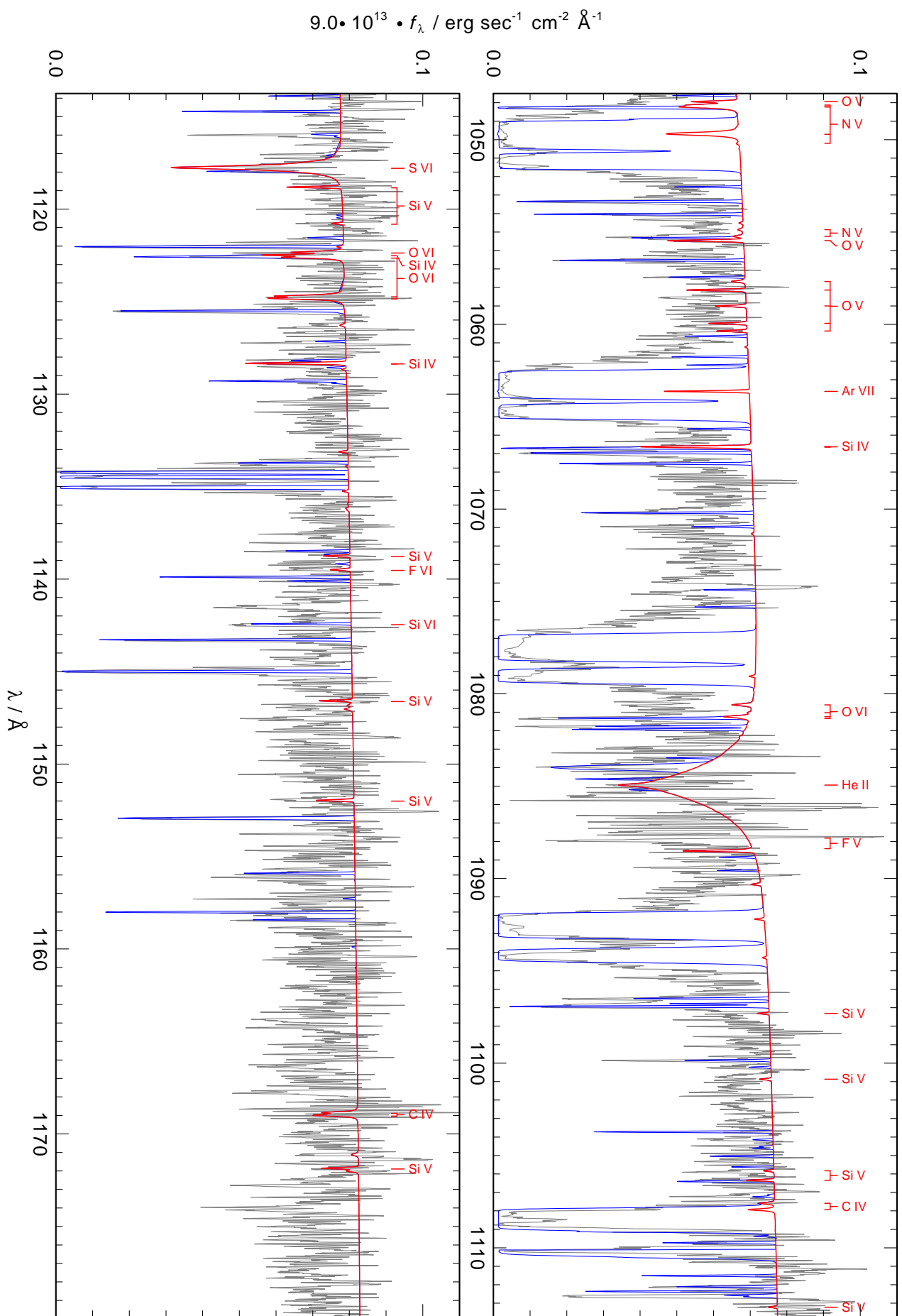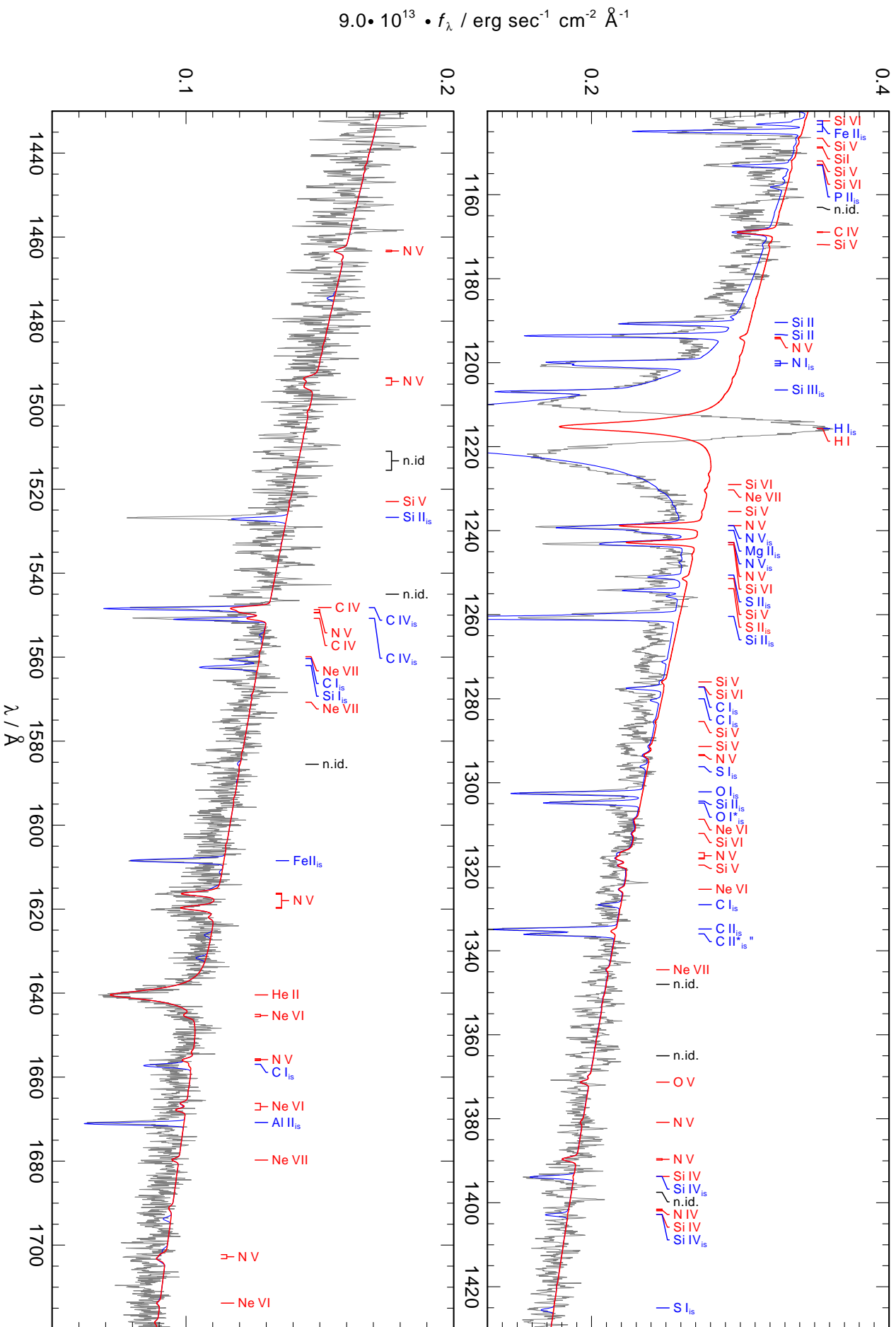**Fig. 3.** Continued.

Fig. 4. Same as Fig. 1 for HS 2209+8229.

Fig. 4. Continued.

Fig. 5. HST/COS spectrum of K 1−27 (gray) compared with final synthetic spectra (red: pure stellar, blue: combined stellar and interstellar). The locations of photospheric (red) and interstellar (blue) lines reproduced by the synthetic spectrum are marked.
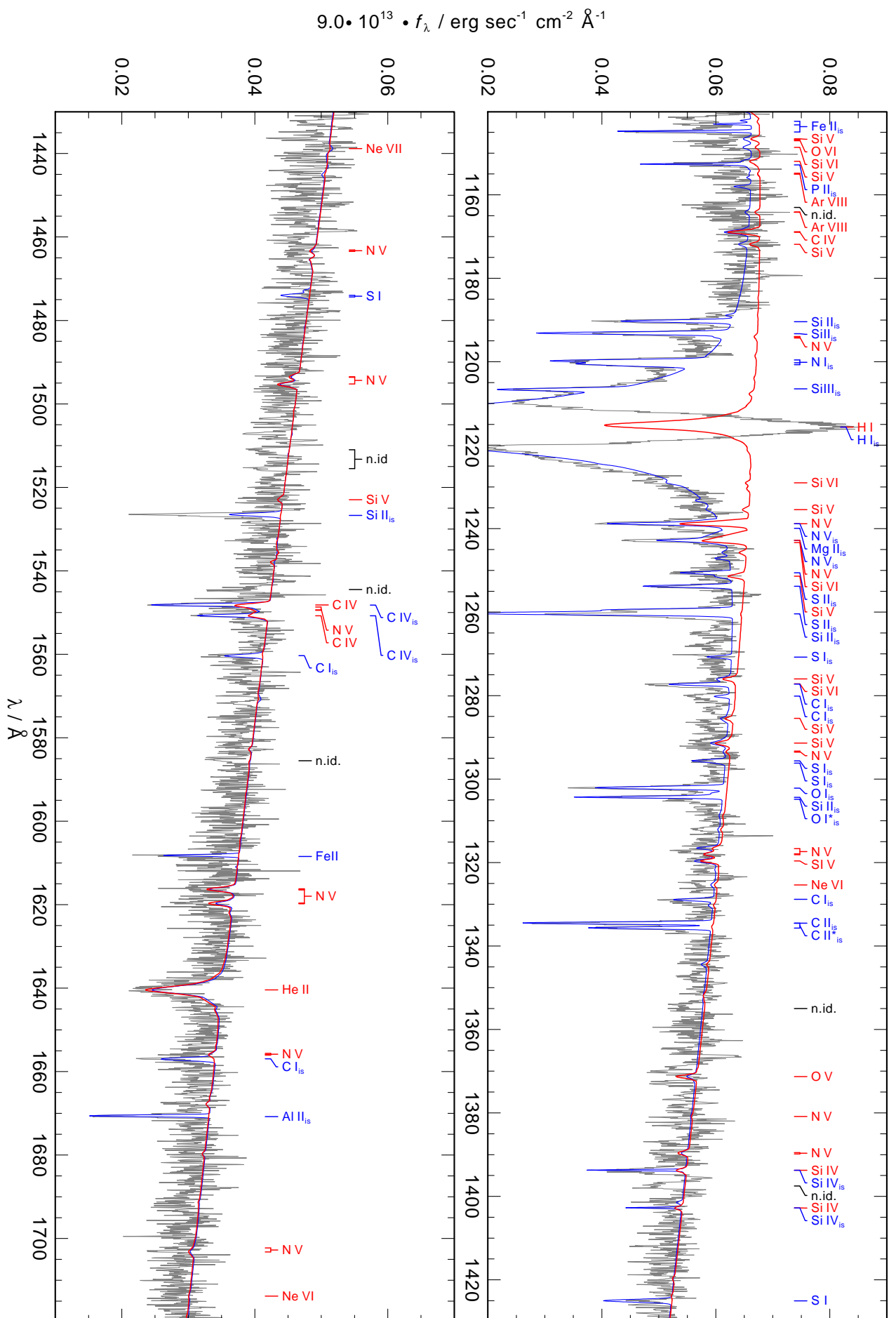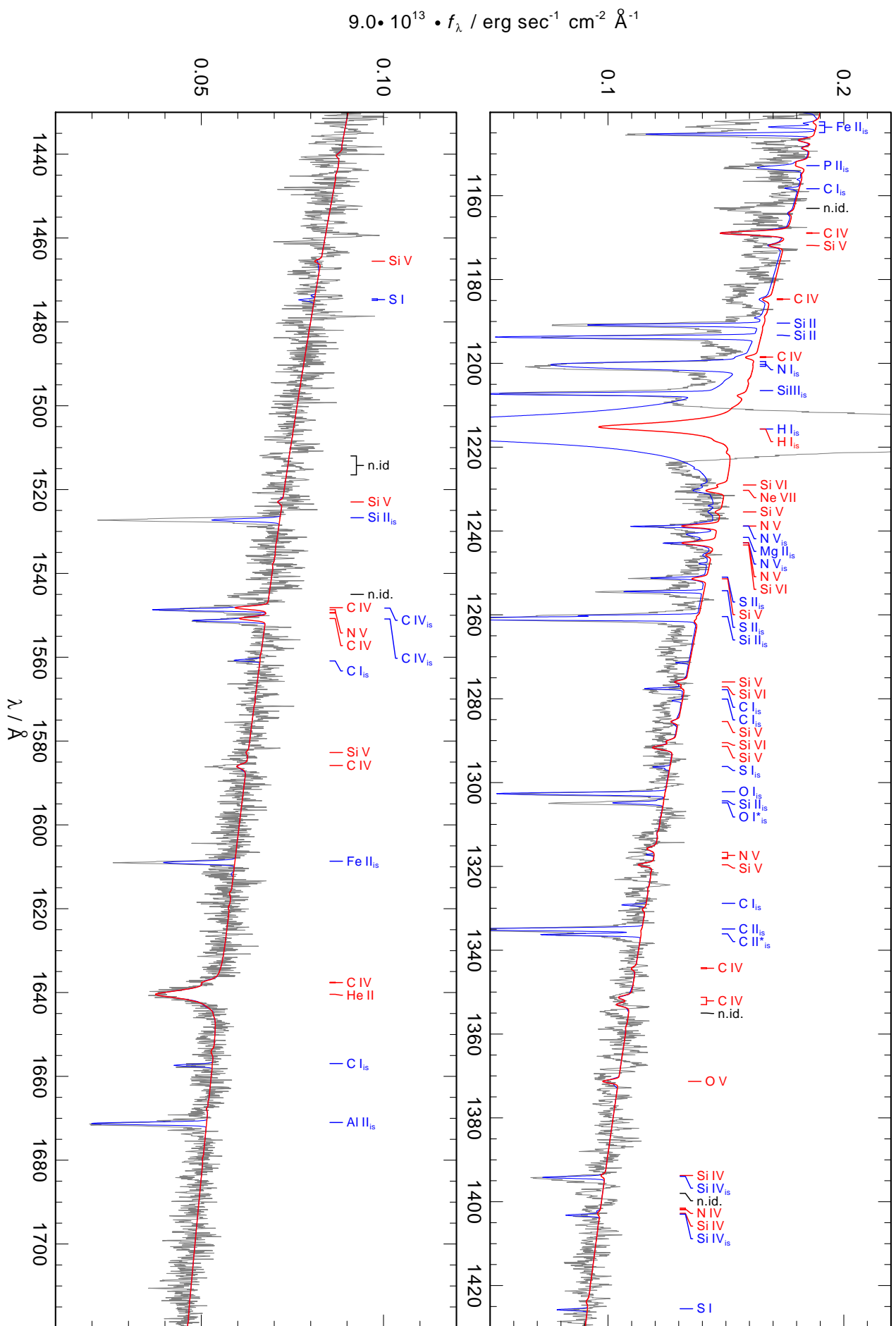
Fig. 6. Same as Fig. 5 for LoTr 4.
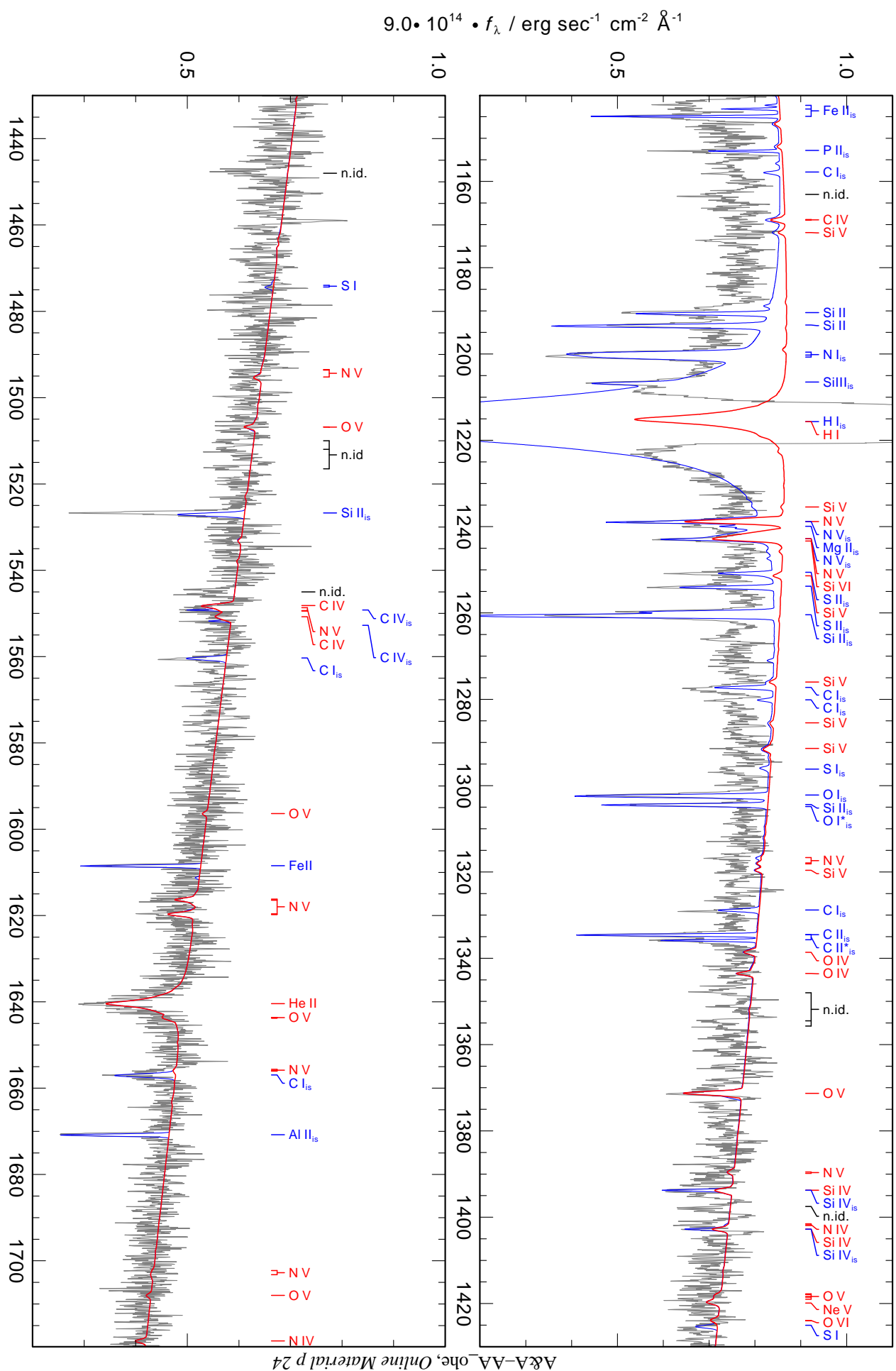
Fig. 7. Same as Fig. 5 for HS 1522+6615.

**Fig. 8.** Same as Fig. 5 for HS 2209+8229.

Table 1. Statistics of the model atoms used in our TMAP calculations.

| | T_{eff} | | | | | |
| | > 110 kK | | | ≤ 110 kK | | |
ion	NLTE	LTE	lines	NLTE	LTE	lines
H I	10	6	45	10	6	45
H II	1	–	–	1	–	–
He I	5	98	3	5	98	3
He II	14	18	91	14	18	91
He III	1	–	–	1	–	–
C III	13	54	32	13	54	32
C IV	14	44	35	14	44	35
C V	1	0	0	1	0	0
N III	1	65	0	1	65	0
N IV	16	78	30	16	78	30
N V	14	48	35	14	48	35
N VI	1	0	0	1	0	0
O IV	18	76	39	18	76	39
O V	17	109	35	17	109	35
O VI	14	48	33	14	48	33
O VII	1	0	0	1	0	0
F V	1	10	0	1	10	0
F VI	6	6	0	6	6	0
F VII	2	4	0	2	4	0
F VIII	1	0	0	1	0	0
Ne IV	0	0	0	2	39	0
Ne V	14	80	18	14	80	18
Ne VI	14	17	30	14	17	30
Ne VII	15	94	27	15	94	27
Ne VIII	14	90	35	1	0	0
Ne IX	1	0	0	1	0	0
Si IV	12	11	24	12	11	24
Si V	25	0	59	25	0	59
Si VI	45	195	193	45	195	193
Si VII	1	0	0	1	0	0
P IV	15	36	9	15	36	9
P V	18	7	12	18	7	12
P VI	1	0	0	1	0	0
S V	23	87	47	23	87	47
S VI	25	12	25	25	12	25
S VII	1	0	0	1	0	0
Ar V				1	359	0
Ar VI	1	183	0	14	170	16
Ar VII	40	112	130	40	112	130
Ar VIII	13	28	24	13	28	24
Ar IX	1	0	0	1	0	0
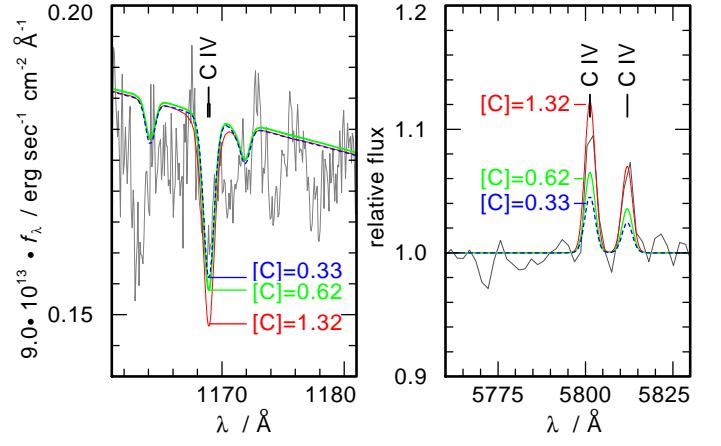
Fig. 21. Determination of the C abundance of HS 1522+6615. C IV lines are compared with models with different C abundances as indicated by the labels.
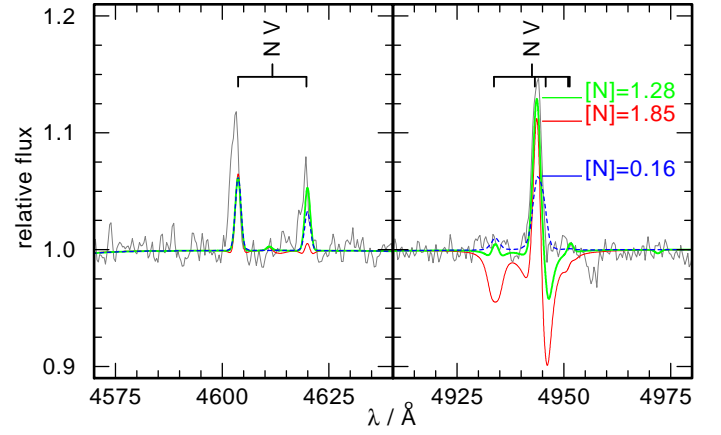
Fig. 22. Determination of the N abundance of K 1−27. N V lines in the EFOSC2 observation are compared with models with different N abundances as indicated by the labels.
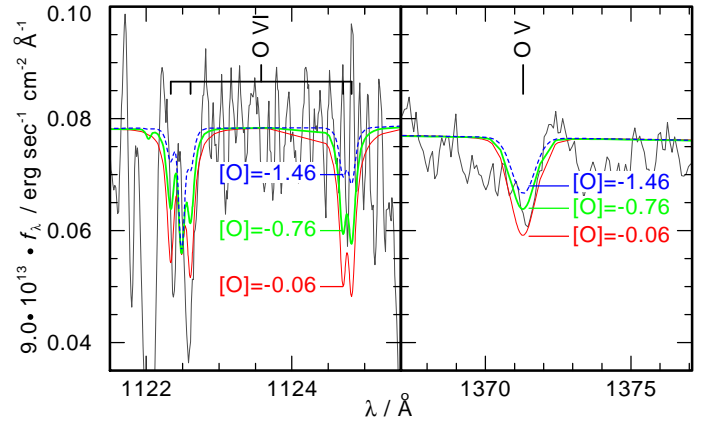
Fig. 23. Determination of the O abundance of HS 2209+8229. O V and O VI lines are compared with models with different O abundances as indicated by the labels.
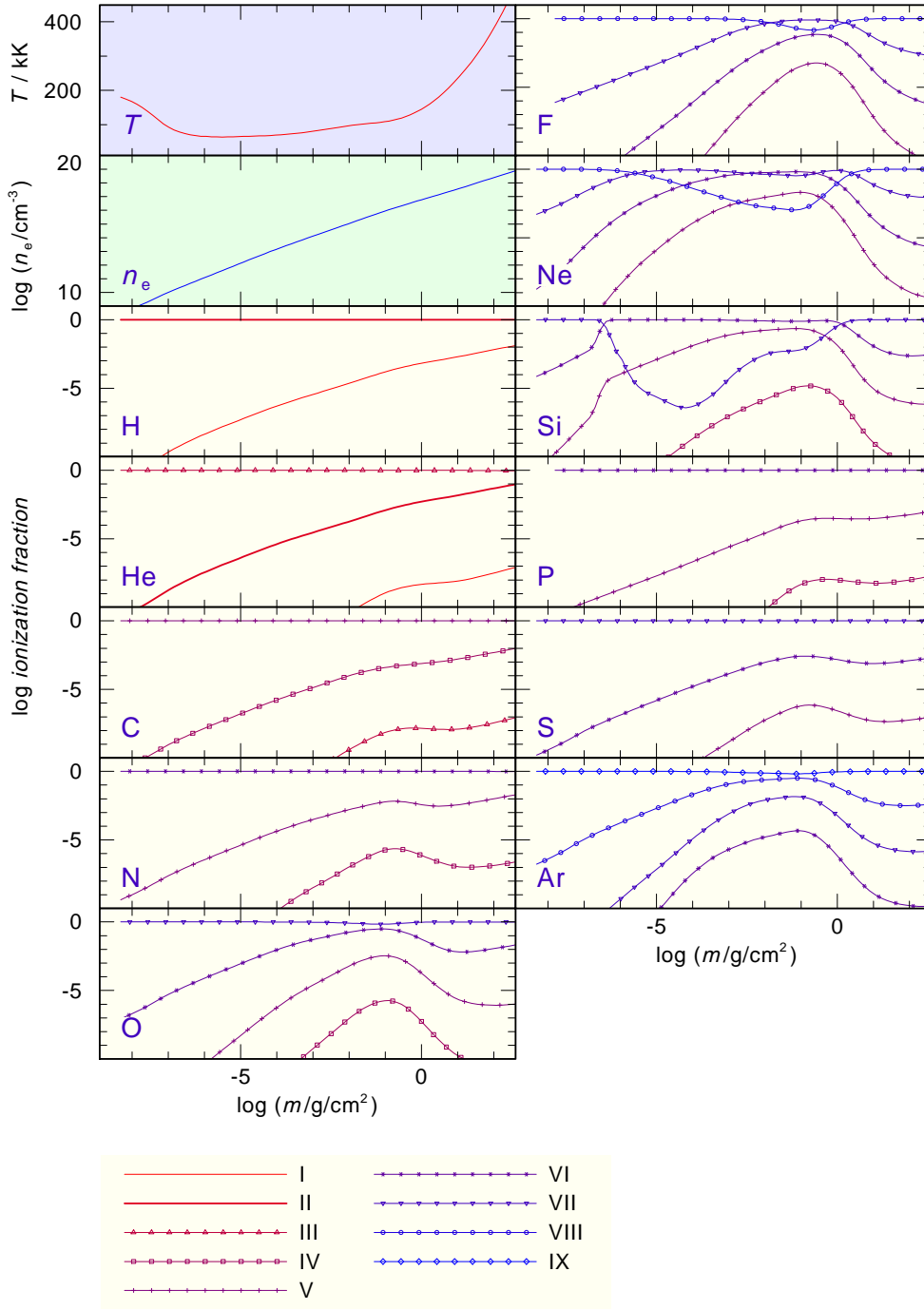
Fig. 9. Temperature, electron density stratification, and ionization fractions of all elements in our final model of K 1−27.
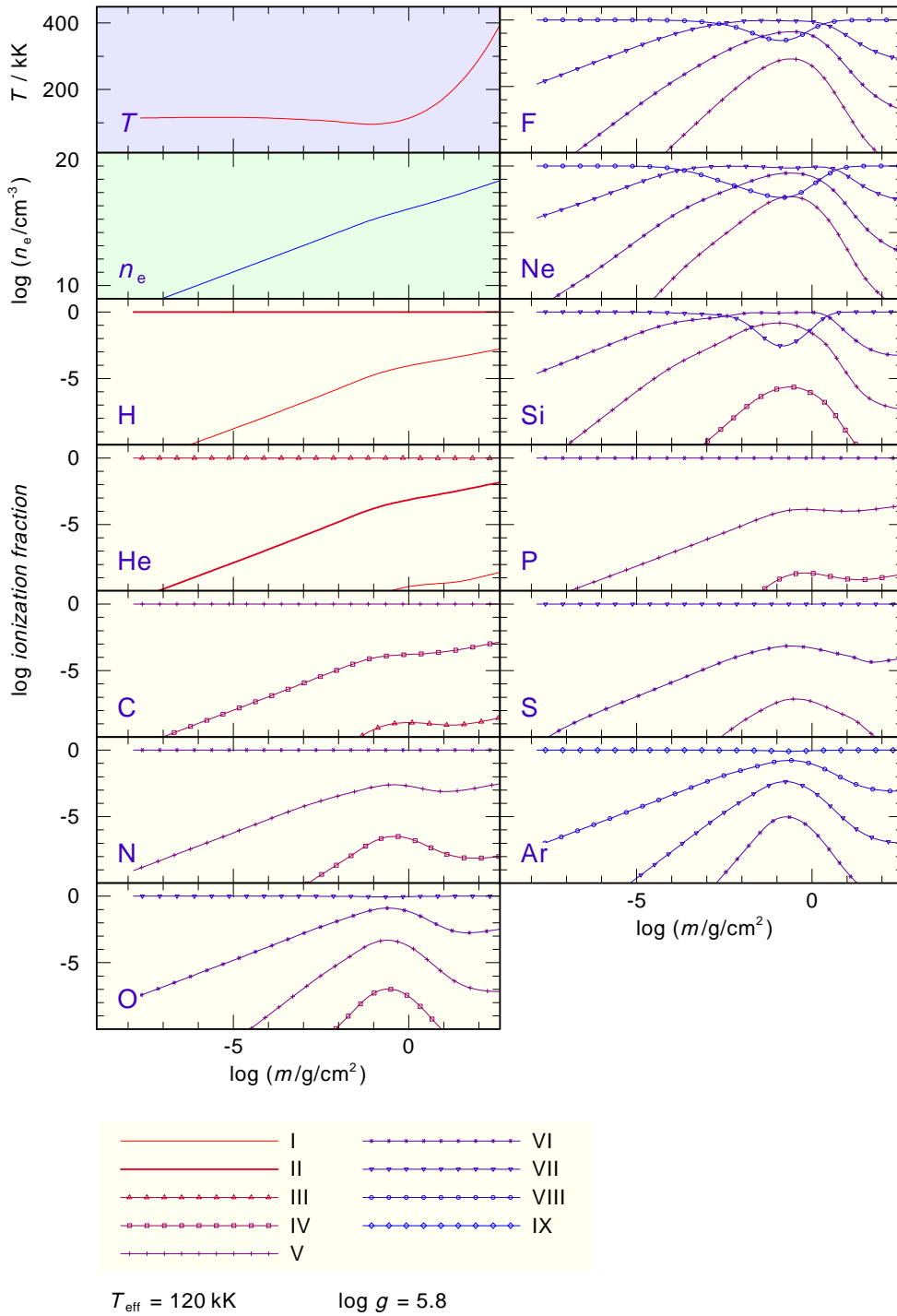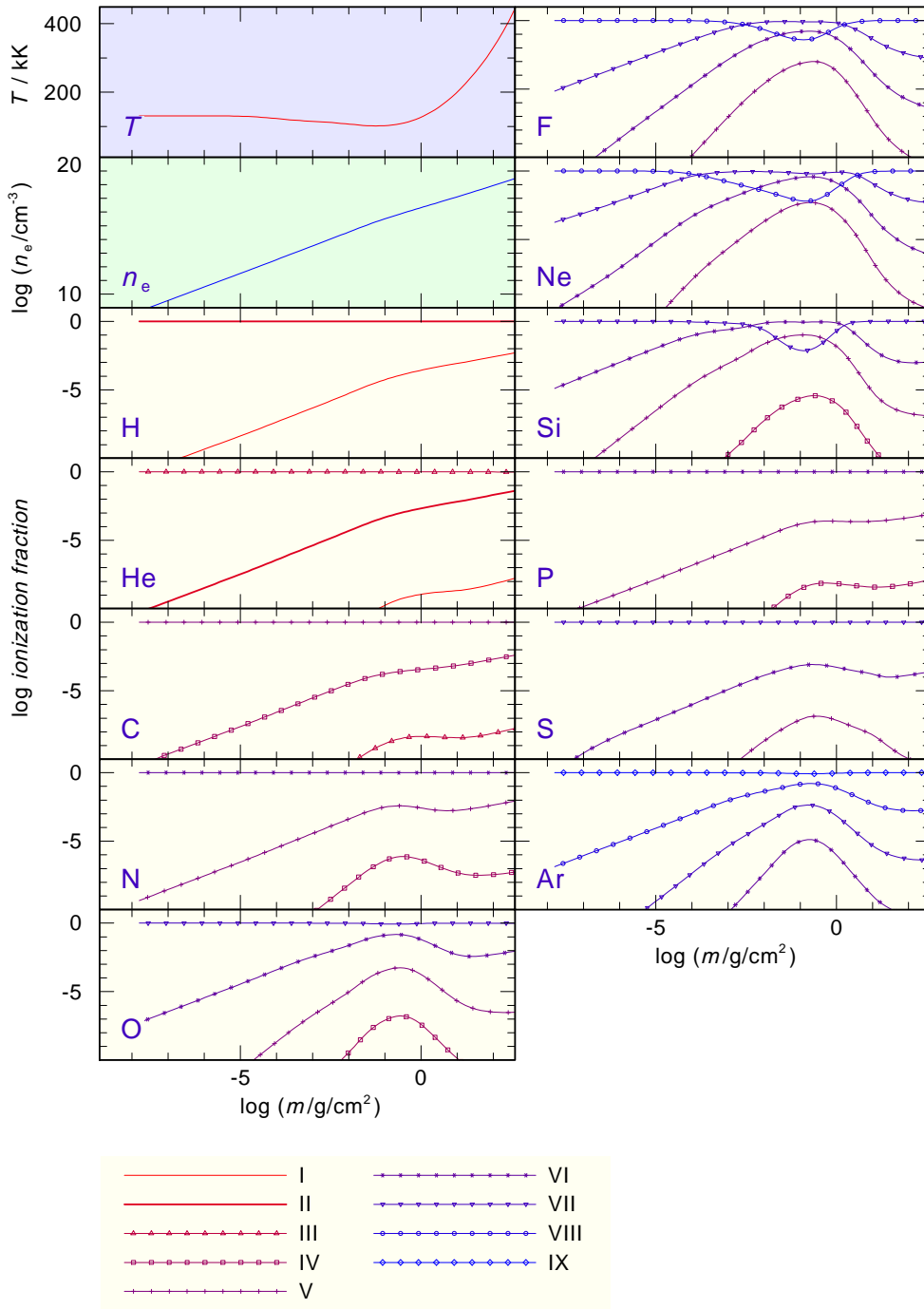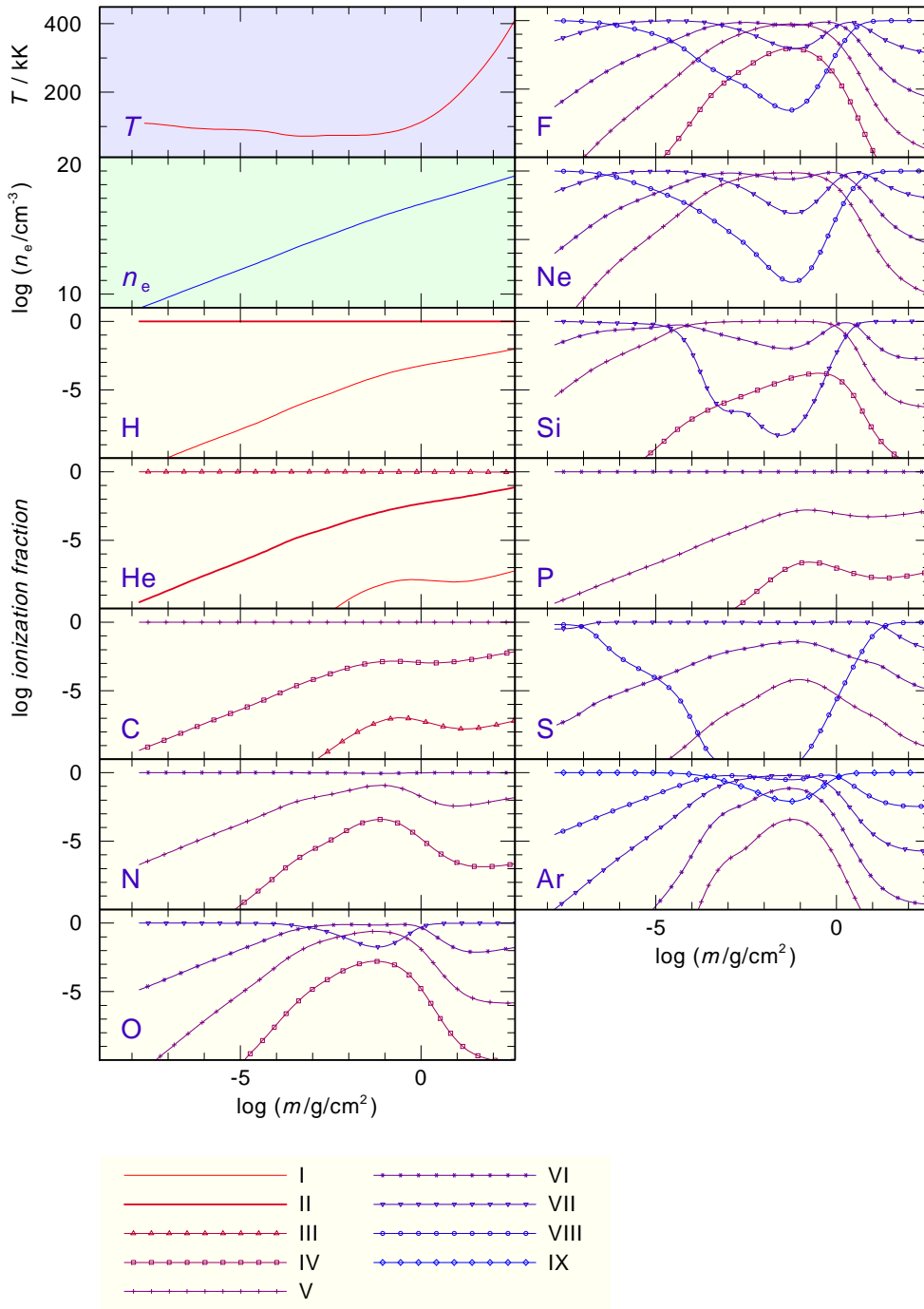
Fig. 10. Like Fig. 9, for LoTr 4.

$T_{\text{eff}} = 130$ kK $\log g = 5.9$

Fig. 11. Like Fig. 9, for HS 1522+6615.

Fig. 12. Like Fig. 9, for HS 2209+8229.